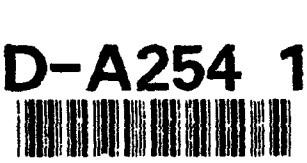

(2)

MATERIALS

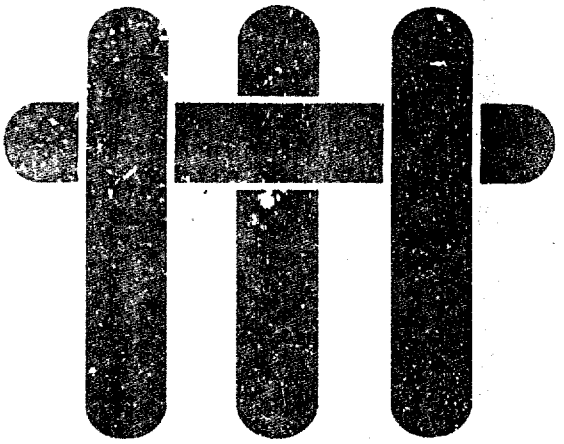

Effect of Surface Forces on the Rheology of Particle-Liquid Systems and the Consolidation of Ceramic Powders

Second Annual Report and Technical Reports 4, 5, 6 and 7

February 1, 1991-January 31, 1992

Office of Naval Research

Grant No. N00014-90-J-1441

Fred F. Lange and Dale S. Pearson

Principal Investigators

Materials Department
University of California
Santa Barbara, CA 93106

REPORT DOCUMENTATION PAGE

Form Approved
OMB No. 0705-0188

1. AGENCY USE ONLY (Leave blank)	2. REPORT DATE	3. REPORT TYPE AND DATES COVERED
	910131	ANNUAL REPORT 2/1/91-1/31/92

4. TITLE AND SUBTITLE

"EFFECT OF SURFACE FORCES ON THE RHEOLOGY OF PARTICLE-LIQUID SYSTEMS AND THE CONSOLIDATION OF CERAMIC POWDERS"

5. FUNDING NUMBERS

N00014-90-J-1441

6. AUTHOR(S)

FRED F. LANGE
DALE S. PEARSON

7. PERFORMING ORGANIZATION NAME(S) AND ADDRESS(ES)

MATERIALS DEPARTMENT
COLLEGE OF ENGINEERING
UNIVERSITY OF CALIFORNIA
SANTA BARBARA, CA 93106

8. PERFORMING ORGANIZATION REPORT NUMBER

9. SPONSORING/MONITORING AGENCY NAME(S) AND ADDRESS(ES)

OFFICE OF NAVAL RESEARCH
MATERIALS DIVISION
800 NORTH QUINCY STREET
ARLINGTON, VA 22217-5000

10. SPONSORING/MONITORING AGENCY REPORT NUMBER

11. SUPPLEMENTARY NOTES

12A. DISTRIBUTION/AVAILABILITY STATEMENT

12B. DISTRIBUTION CODE

13. ABSTRACT (Maximum 200 words)

More reliable ceramics require improved processing reliability. Heterogeneities bought with powders and those inadvertently introduced during processing as well as non-uniform and undefined phase distributions contribute to unreliable processing. Colloidal powder treatments can eliminate many heterogeneities and ensure more uniform phase distributions. To ensure that new heterogeneities are not introduced, colloidally treated powders must be piped, as slurries, directly to a die cavity. Slurry consolidation methods based on particle partitioning, e.g., pressure filtration and centrifugation are emphasized in this review. Interparticle potentials play a dominant role in governing the slurry viscosity, maximum particle packing density and the rheology of the consolidated body. These roles will be reviewed with the objective to understand how damage free bodies can be consolidated from slurries to increase the structural reliability of ceramics and their composites.

14. SUBJECT TERMS	15. NUMBER OF PAGES
Ceramics, Heterogeneities, Slurry, Colloidal Powder	76
	16. PRICE CODE

17. SECURITY CLASSIFICATION OF REPORT	18. SECURITY CLASSIFICATION OF THIS PAGE	19. SECURITY CLASSIFICATION OF ABSTRACT	20. LIMITATION OF ABSTRACT
UNCLASSIFIED	UNCLASSIFIED	UNCLASSIFIED	

M A T E R I A L S

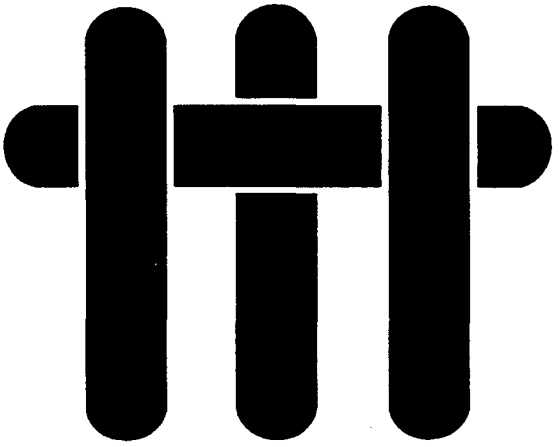

Technical Report Number 4

Influence of Interparticle Forces on the Rheological Behavior of Pressure Consolidated Ceramic Particle Slurries

B. V. Velemakanni, F. F. Lange, F. C. Zok and D. S. Pearson

Office of Naval Research

Grant No. N00014-90-J-1441

Fred F. Lange and Dale S. Pearson

Principal Investigators

Materials Department
University of California
Santa Barbara, CA 93106

Influence of Interparticle Forces on the Rheological Behavior of Pressure Consolidated Ceramic Particle Slurries

Bhaskar V. Velamakanni, Fred F. Lange, Frank C. Zok and Dale S. Pearson

Materials Department, University of California, Santa Barbara, CA 93106

The stress relaxation behavior of alumina powder compacts, consolidated from aqueous slurries by pressure filtration, is reported. The interparticle forces were controlled, prior to consolidation, by changing the pH from 3 to 9 and by adding different amounts of salt (0.1 to 2.0 M NH4Cl) to pH 4 slurries. Disc shaped bodies were rapidly compressed by 2 % and the resulting relaxation data was determined as a function of time. For bodies formed at pH ≤ 4 without added salt, the stress relaxation behavior consisted of an irreproducible mixture of plastic and elastic response. The initial stress and the stress retained after long relaxation periods was highest for bodies formed with pH 9 slurries. At pH 4, the initial stress increased with the addition of 0.1 to 0.5 molar salt, but the bodies behaved plastically with more than 90 % of the initial stress relaxing within a short period. These results are consistent with a short-range, repulsive interparticle force that lowers the attractive force between particles. They also suggest that interparticle forces in consolidated bodies can be controlled in a way that should prove useful in preventing damage that occurs during processing and reforming operations.

I. Introduction

Colloidal methods for processing ceramic powders offer the potential for producing more reliable products.[1] An effective procedure consists of mixing the powder with a liquid and then adjusting the interparticle potential to produce strongly-repulsive forces. Under these conditions, agglomerated particles that are broken apart will remain separated, and other heterogeneities (partially sintered agglomerates, inclusions, etc.) greater than a desired size can easily be removed from by sedimentation or filtration. Once the heterogeneities are removed, the interparticle forces can made attractive so that a weak network is formed. In this way particle size segregation in single phase powder systems or phase separation in

multi-phase powder systems is prevented. To avoid reintroducing heterogeneities, the slurry should be formed directly into the desired engineering shape.

It has been shown that when the interparticle forces are too strongly attractive, particles cannot easily be packed to their highest packing density.[2,3] Furthermore, the particle packing density is very pressure sensitive [2], and the consolidated body is elastic-like and very prone to cracking after the pressure is removed.[2, 4] When the interparticle forces are repulsive, high packing densities can be achieved at practical pressures; [2] however, mass segregation can occur prior and during consolidation.[5] In addition, after consolidation the bodies consolided from dispersed slurries can flow and lose their shape.

We have recently [6] shown that weakly attractive interparticle potentials can be achieved in aqueous Al_2O_3 slurries. The method begins conventionally by adjusting the pH to produce highly repulsive interparticle forces (pH $\leq$ 4) in agreement with the Derjaguin-Landau-Verwey-Overbeek (DLVO) theory. It was shown that when an indifferent electrolyte was added to a highly dispersed slurry, a very short-range repulsive potential was discovered, as counter ions diminished the magnitude of the long-range repulsive electrostatic potential. This short-range interparticle potential is currently believed to be due to a hydrated layer similar to that found for mica surfaces [7,8], and for clay surfaces [9]. Viscosity and yield stress measurements indicate [6] that beyond a certain salt concentration ($\approx$ 0.1 molar, sufficient to lower the repulsive barrier so that particles can coagulate), an attractive network is formed with a strength that increases with salt content. At a higher concentration (where the electrostatic repulsive potential is negligibly small) the network strength is no longer increased with further additions of salt. The strength of these networks as judged by viscosity, yield stress, and packing pressure measurements, is considerably lower than networks formed at the isoelectric point (pH = 9). From these observations, it was concluded that particles in the salted slurries are prevented from contacting each other by the short range potential described above.

These findings are in disagreement with the DLVO theory which predicts that either adding high concentrations of electrolyte or changing the pH to the isoelectric point will produce the same attractive Van der Waals potential. To distinguish the two cases we call networks formed by adding salt at low pH coagulated, and networks formed by changing the pH to the isoelectric point flocced.

Unlike the flocced slurry (with or without salt) where particles form a very strong network, the short-range, repulsive interparticle forces in a coagulated slurry

form a weak, but non-touching network and hence act as a 'lubricant' that allows particles to easily rearrange and pack to a high density.[6] Because of this, coagulated slurries can be packed to a high densities by centrifugation without particle segregation.[10] Centrifugation of two different coagulated slurries was recently used in a unique way to fabricate a layered toughened material.[11] In addition, unlike dispersed slurries, Al_2O_3 bodies formed from coagulated slurries retain their shape after consolidation, but can be reshaped by plastic flow. In many respects, coagulated slurries and the bodies they form have rheological characteristics similar to clay systems.

The purpose of the present work is to characterize the rheological behavior of water saturated bodies formed from dispersed, flocced and coagulated Al_2O_3 slurries. Because the stresses that are generated in deforming these bodies are high and conventional shear rheological instruments are not currently equipped to study the behavior of saturated powder compacts, stress relaxation experiments were performed with a servo-hydraulic testing machine.

I. Experimental Methods

(1) Slurry Preparation

Aqueous slurries containing 20 vol.% α-alumina powder [a] (0.2 μm mean particle diameter) were used in this study. All slurries were prepared by first dispersing the powder in deionized water at pH 4. At this pH, the zeta potential of alumina is sufficiently large to keep the particles dispersed. A high shear-field, obtained by immersing an ultrasonic horn in the slurry, was used to break apart agglomerated particles. The pH was then adjusted with analytical grade HNO_3 or NH_4OH, and if salt was used, analytical grade NH_4Cl .

(2) Pressure Filtration

Pressure filtration was used to prepare the consolidated ceramic bodies. A predetermined volume of slurry was poured into a cylindrical filtration die 2.54 cm in diameter to make consolidated bodies ~ 1 cm thick after filtration was complete.[2] Pressure of 14.6 MPa was applied to the plunger with an automated hydraulic press. A portion of each slurry was consolidated to determine packing densities as described elsewhere [6]. The average particle packing densities in consolidated bodies

[a] Sumitomo Chemical Co., New York, Grade APK-50

made from dispersed (pH <4) slurries and flocced (pH 8 to 9) slurries are 62% and 54% of theoretical, respectively. As described elsewhere [5], the packing density of the consolidated bodies decreased gradually from 62% to 54% as the pH increases from 5 to 8. For the case of coagulated slurries, the packing densities were 62%. While removing samples from the die and during subsequent handling, extreme care was exercised to minimize any distortion. After measuring the dimensions, the saturated bodies were immediately sealed in a zip-lock, plastic bag containing a moist paper towel. The presence of the towel ensure that there was sufficient humidity in the bag to prevent the body from drying during testing and storage. [Although stress relaxation experiments were performed within hours after the samples were sealed in a bag, we determined that the bodies would retain their rheological characteristics for at least one week.]

(3) Stress Relaxation Measurements

The stress relaxation experiments were performed with a servo hydraulic testing machine. The testing machine [b] was equipped with a microprofile processor for controlling crosshead displacement and a personal computer [c] for data acquisition. The machine was equipped with a 1000 lb (4448 N) stationary load cell and the machine was controlled with the following cartridges: ±200 lb (890 N) and ±500 lb (2224 N) for load, ±1.27 cm and ±0.4064 cm for displacement. Two flat compressive platens were used to compress the cylindrical specimen contained within the plastic bag. All the experiments were performed with the machine in displacement control mode. Data on time, load and displacement was acquired at 9 points/sec. After the consolidated body was placed on the bottom platen, the crosshead was carefully raised to bring the top portion of the consolidated body in contact with the upper platen. A small compressive load of 0.5 to 2 N was applied to the sample to ensure that both the upper and lower platens were in good contact with the specimen.

An experiment consisted of applying a step compressive strain at the rate of 1.7×10^{-3} m/sec until a displacement equivalent to a 2 % linear strain. The nominal time to accomplish this was 0.12 seconds after which the crosshead was stopped. Stress was calculated assuming that the area of the specimen did not change during the application of the 2 % strain. At least two consolidated bodies were fabricated

[b] (testing machine, model etc)
[c] IBM PC-AT

and tested for each pH and/or salt concentration. The experiment was terminated when the compressive load relaxed to either zero or a to an apparent constant value. Some experiments were conducted by applying further strains of 2% to the same specimen.

III. Results

A preliminary analysis indicated that the data could not be described by a single exponential function. The results we present consist of two experimentally determined parameters: the peak stress, σ_o, obtained at the end of the initial, rapid straining period, and the final stress, σ_s, obtained from the period where the stress appears constant. The slow data acquisition also resulted in considerable scatter (~ ± 25 %) in the determination of σ_o.

(1) Influence of pH

The first series of stress relaxation experiments were made on the consolidated bodies made from dispersed and flocced slurries. Although the stress relaxation behavior of samples made from flocced slurries was reproducible, the behavior of consolidated bodies made from dispersed slurries (at any pH ≤ 4.5) was erratic. Neither the shape of the stress relaxation curve nor the values of σ_o and σ_s were reproducible. The rheological behavior ranged from viscous flow (small σ_o and $\sigma_s \rightarrow 0$) to elastic-like behavior (large σ_o and $\sigma_s > 0$). A possible reason for this variation will be discussed below.

Reproducible data could be obtained for bodies prepared from dispersed slurries by adding as little as 0.1 M NH_4Cl to the slurry prior to consolidation. Previous experiments [6] showed that this amount of NH_4Cl was the minimum amount needed to produce an attractive particle network. Adding salt neither effected the stress relaxation behavior nor final packing density of bodies prepared from slurries at pH values near the isoelectric point. [6]

Figure 1a and 1b show the average peak stress (σ_o) and the ratio of the initial to final stress (σ_s/σ_o) as a function of pH for bodies consolidated with slurries containing 0.1 M NH_4Cl. These data show a transition between plastic behavior (small σ_o, $\sigma_s/\sigma_o \rightarrow 0$) to elastic-like behavior (large σ_o, $\sigma_s/\sigma_o > 0$) between a pH of 4 to 5.

(2) Influence of Electrolyte Concentration

In other experiments [12] we report that the viscosity and yield stress increases with increasing salt concentration in coagulated slurries. In the present experiments we determined that a similar behavior is found for consolidated bodies. Although there is large scatter in our experimental observations, the average value of σ_o increases with salt concentration between 0.1 M to 0.5 M. It was also observed that the ratio of relaxed stress increased from ≈ 0 to 0.1 ± 0.05 over the same range of salt concentration (0.1 M to 0.5 M) and remains constant for salt concentrations ≥ 0.5 M. These data confirm that the strength of the particle network is enhanced when the salt concentration exceeds 0.1 M, but over 90 % of the peak stress is quickly relaxed.

(3) Sequential Straining Experiments

Figure 3a shows the relaxation behavior of a body consolidated from a slurry at pH 3.8 and containing 0.1 M NH_4Cl. The sample was sequentially subjected to 2 strain cycles of 2 % each. As shown, the relaxation occurs much more rapidly after the second strain cycle. This body was then subjected to a third cycle (not shown), but no stress response was observed. Figure 3b shows the effect of a second strain cycle on the relaxation of a body consolidated from a pH 4 slurry containing 2 M NH_4Cl. Similar to the behavior shown in Fig. 3a, stress relaxation is more rapid after the first cycle. These observations show that the behavior is history dependent, becoming more plastic in subsequent strain cycles. Figure 4 shows the effect of repeated strain cycles on the stress relaxation behavior of a consolidated body at pH 6 and containing 0.1 M NH_4Cl. After the initial 2% strain, the consolidated body relaxes to a saturation stress about 30% of the peak stress. However, upon repeated straining the residual stress continues to increase - the body exhibits strain hardening. The same behavior was observed for samples subjected to as many as 16 strain cycles of 2% each.

(4) Influence of Aging

The effect of aging was investigated for bodies made from both dispersed and coagulated slurries after they had been already subjected to one cycle of strain. After the initial stress relaxation experiment, the body (still contained within its plastic bag) was carefully removed from the testing machine and left undisturbed for a predetermined period. Later, the body was tested again to determine its stress relaxation behavior. Although, the rheology of the consolidated bodies made from coagulated slurries were still plastic after 7 days, bodies made from dispersed slurries (pH 4, without salt) that were very plastic during the first strain cycle became elastic-

like after only 24 hrs of aging. Bodies consolidated from coagulated slurries that had been subjected to repeated strain cycles until no stress response was observed (e.g., a specimen similar to that shown in Fig. 3a) remained plastic after aging.

IV. Discussion

The data presented above clearly shows that the maximum stress achieved during rapid straining and the amount of stress relaxation strongly depends on interparticle potentials. Several basic relations are evident. First, bodies formed with coagulated slurries (and some with dispersed slurries) quickly relax their stress after rapid straining, whereas the stress in bodies formed with flocced slurries does not completely relax. In contrast, the rather cohesive particle networks formed from flocced slurries can support relatively large amounts of stress for long periods despite their lower particle packing density. Second, it appears that the particle networks of some bodies formed from dispersed slurries become cohesive during either consolidation or aging to behave similarly as flocced networks.

(1) Interparticle Potentials, Particle Networks and Plastic Flow

Figure 5 schematically illustrates the expected interparticle potential as a function of particle separation for the three types of slurries we used to form bodies. The first two Figures, 5a and 5b, are for flocced and dispersed particles. There interaction potentials are expected to conform closely to the well known DLVO theory. They apply to materials near the isoelectic point (pH range of 7 to 9) and at low pH (< 4), where the density of positive surface sites is low and high, repectively.

Particles in a flocced slurry (Fig. 5a) are expected to be in elastic contact. This contact and the resulting friction between particles will resist particle rearrangement during pressure consolidation. However, once consolidated to a given packing density, the relatively cohesive network should support a stress up to the yield point.[13] Beyond yield, particle rearrangement is expected to produce either an increased packing density if liquid is expelled[14] or plastic flow if the liquid volume in the compact remains constant. Unless constrained with hydrostatic pressure, one generally exceeds the fracture strength of flocced bodies, consolidated at high pressures, prior to plastic flow.

Particles in a dispersed slurry repel one another. When pushed together during consolidation, their mutual repulsive force (see Fig. 5b) will act as a 'lubricant' easing rearrangement and leading to a high packing density that is

relatively pressure insensitive. If the repulsive interparticle potential persists after particle packing, then the body is expect to still flow although with a much higher viscosity relative to the slurry. In this way it can relieve any energy stored when pressure was applied. On the other hand, once a stable packing arrangement has been achieved, the applied force between particles can be increased to exceed the repulsive interparticle force if the body is constrained from flow (e.g., within a die cavity). If this occurs, the particles will be 'pushed' into the primary minimum of the van der Waals potential. Under these conditions, the particles will form a touching, strongly cohesive network, and with flow properties similar to that described above for flocced bodies.

Kuhn et al [13] have shown that when pressure is applied to a powder compact, the force between pairs of particles within a network ranges between zero and a maximum value. That is, some particles are not stressed and others support a larger than average portion of the applied pressure. Thus, only a fraction of the particles in a dispersed slurry are expected to be pushed into the primary minimum. Likewise, a fraction of the particles will still be on the repulsive side of the DLVO potential. Thus, the rheology of a body formed from a dispersed slurry will depend on the fraction of particles in the primary minimum which should be a strong function of the consolidation conditions (magnitude of applied pressure, period of pressure application, etc.).

Other effects, generally attributed to aging, can also cause initially repulsive particles to become attractive. For example, when alumina is stabilized with a low pH, the pH drifts presumably due chemical reactions of the acidic water with the particles themselves. Bodies consolidated from initially dispersed slurries could do the same, and thus dramatically change their behavior.

The coagulated slurry is described by a combination of interparticle potentials consisting of the van der Waals attractive potential, a small residual electrostatic repulsive potential, and we believe a short-range, repulsive, hydration potential (see Fig. 5c). Israelachvili and Adams [15] were the first to discover the hydration potential during force measurements between smooth mica surfaces in aqueous media. They observed that surfaces in dilute electrolyte solutions (for example, $KNO_3 < 10^{-4}$ M) obey the DLVO theory. However, at higher salt concentrations, in addition to the attractive van der Waals and diffuse, double-layer repulsive forces, an additional repulsive force was observed when the surfaces were close to touching. Later, this force was termed a "hydration" force. Certain cations such as Li^+, Na^+, K^+, Mg^{2+} bind to the negatively charged mica surfaces and become hydrated. This gives rise to

a short range repulsive force due to the energy needed to dehydrate the bound cations. [7,8] The strength and range of hydration forces increased with the hydration number of the cations. The magnitude of hydration force seems to decrease exponentially with a characteristic decay length of 1.0±0.2 nm. Measurements between interacting micro-rough surfaces is exponentially repulsive below 4 to 6 nm. [16] At separations near 2 nm, the repulsive pressure between surfaces can exceed 10 MPa. [16] Such repulsive hydration forces between surfaces are not a part of the conventional DLVO model.

A recent study by Velamakanni et al. [6] examined the behavior of alumina slurries at pH ≤ 4 and in the presence of Cl^-, Br^-, I^-, or NO_3^- cations that can interact with positive sites like $AlOH_2^+$. Because of the lower viscosity and yield stress that these materials have relative to alumina at the isoelectric point, it is believed that hydration layers are present. However, because of decreasing number of positive sites as the pH approaches the point of zero charge (pH ≈ 8.5), hydration layer should become less important for these materials. All of the observations in their study are consistent with the presence of short-range hydration repulsion layer that prevents particles from falling into the primary minimum required to produce the cohesive, touching network predicted by DLVO theory. A short range repulsive force would predict that the particles are in a potential well of more modest depth that produces a weakly attractive network which we call a coagulated network.

Although particles in a coagulated slurry attract one another, if pushed together during consolidation, their mutual, repulsive force can act as a lubricant to ease rearrangement and lead to a relatively pressure insensitive, high packing density similar to that discussed for the dispersed slurry. But unlike the purely repulsive particles in a dispersed slurry, particles within a consolidated, coagulated body are attracted to each other. Thus, the yield stress of a consolidated, coagulated body is expected to be proportional to the depth of the potential well.

The stress relaxation data presented here are consistent with the interparticle potentials described in Fig. 5. When the long-range interparticle potentials persists after consolidation, bodies formed from dispersed slurries undergo plastic flow to relieve any stress stored during rapid straining. On the other hand, it appears that some fraction of particles could be pushed into their primary minimum, leading to behavior similar to that found for flocced bodies. The stress relaxation data strongly suggests that the short-range repulsive potential is effective during consolidation and is unaffected by aging. The stress relaxation behavior of coagulated bodies subjected to repeated strain cycles (Fig. 4) further suggests that some of the particles

do form cohesive bonds during pressure consolidation that are broken during each strain cycle. In addition, the increased peak stress with increasing salt content is consistent with the understanding that the particles will are in a deeper potential well that makes their rearrangement more difficult.

(2) Effect of Added Electrolyte on the Development of the Short-Rang Repulsive Potential

In our initial report on the effect of the added electrolyte on dispersed Al_2O_3 slurries, [6] it was hypothesized that the negatively charged, hydrated counterions produced a short-range repulsive potential similar to the hydration potential described by Israelachvili and coworkers [7,8,15-17]. The stress relaxation experiments presented here provide further support for this idea. Namely the addition of ≥ 0.1 M NH_4Cl to dispersed slurries produces either exhibit plastic or elastic flow properties. Because of the small particle separations in consolidated bodies, our observations strongly suggests that the short-range repulsive potential is not present, hidden from our experiments by the long-range repulsive potential, before electrolyte is added.

Acknowledgment: This research was supported by a Grant from the Office of Naval Research under Contract No. N00014-90-J-1441.

5. References

1. F. F. Lange, "Powder Processing Science and Technology for Increased Reliability," J. Am. Ceram. Soc. 72 [1], 3-15 (1989).

2. F. F. Lange and K. T. Miller, "Pressure Filtration: Kinetics and Mechanics," Bul. Am. Ceram. Soc. 66 [10], 1498-1504 (1987).

3. T. J. Fennelly and J. S. Reed, "Mechanics of Pressure Casting," J. Am. Ceram. Soc., 55[5] 882-88 (1972).

4. F. F. Lange, B. V. Velamakanni, and A. G. Evans, "Method for Processing Metal-Reinforced Ceramic Composites," J. Am. Ceram. Soc. 73 [2] 388-93 (1990).

5. B. V. Velamakanni and F. F. Lange, "Effect of Interparticle Potentials and Sedimentation on Particle Packing Density During Pressure Filtration," J. Am. Ceram. Soc. 74 [1] 166-72 (1991).

6. B. V. Velamakanni, J. C. Chang, F. F. Lange, and D. S. Pearson, "New Method for Efficient Colloidal Particle Packing via Modulation of Repulsive Lubricating Hydration Forces," Langmuir 6 [7] 1323-25 (1990).

7. R. M. Pashley, "DLVO and Hydration Forces between Mica Surfaces in Li^+, Na^+, K^+, and Cs^+ electrolyte Solutions: A Correlation of Double-Layer and Hydration Forces with Surface Cation Exchange Properties," J. Colloid Interface Sci, 83, 531-46 (1981).

8. R. M. Pashley and J. N. Israelachvili, DLVO and Hydration Forces between Mica Surfaces in Mg^{2+}, Ca^{2+}, Sr^{2+}, and Ba^{2+} Chloride Solutions," J. Colloid Interface Sci., 97, 446-55 (1984).

9. H. van Olphen, An Introduction to Clay Colloid Chemistry, p 99 John Wiley & Sons, New York, 1977.

10. J. C. Chang, B. V. Velamakanni, F. F. Lange, and D. S. Pearson, "Centrifugal Consolidation of Al_2O_3 and Al_2O_3/ZrO_2 Composite Slurries vs Interparticle Potentials: Particle Packing and Mass Segregation," J. Am. Ceram. Soc. 74 [9] 2201-204 (1991).

11. D. B. Marshall, J. J. Rato, and F. F. Lange, "Enhanced Fracture Toughness in Layered Microcomposites of Ce-ZrO_2 and Al_2O_3," J. Am. Ceram. Soc. (in press).

12. J. C. Chang, F. F. Lange, and D. S. Pearson, "Viscosity and Yield Stress Behavior of Al_2O_3 Slurry Systems as a Function of Interparticle Potenials," to be published.

13. L. T. Kuhn, R. M. McMeeking, and F. F. Lange, "A Model for Powder Consolidation," J. Am. Ceram. Soc. 74 [3] 682-85 (1991).

14. C. P. Cameron and R. Raj, "Better Sintering Through Green-State Deformation Processing," J. Am. Ceram. Soc. 73 [7] 2032-37 (1990).

15. J. N. Israelachvili and G. E. Adams, "Measurement of Forces between Two Mica Surfaces in Aqueous Electrolyte Solutions in the Range 0-1000 nm," J. Chem. Soc. Faraday Trans. 1, 74 , 975-1001 (1978).

16. J. N. Israelachvili and R. M. Pashley, "Molecular Layering of Water at Surfaces and Origin of Repulsive Hydration Forces," Nature, 306 (5940) 249-50 (1983).

17. J. N. Isrealachvili, "Measurements of Hydration Forces between Macroscopic Surfaces," Chemica Scripta, 25, 7-14 (1985).

List of Figures

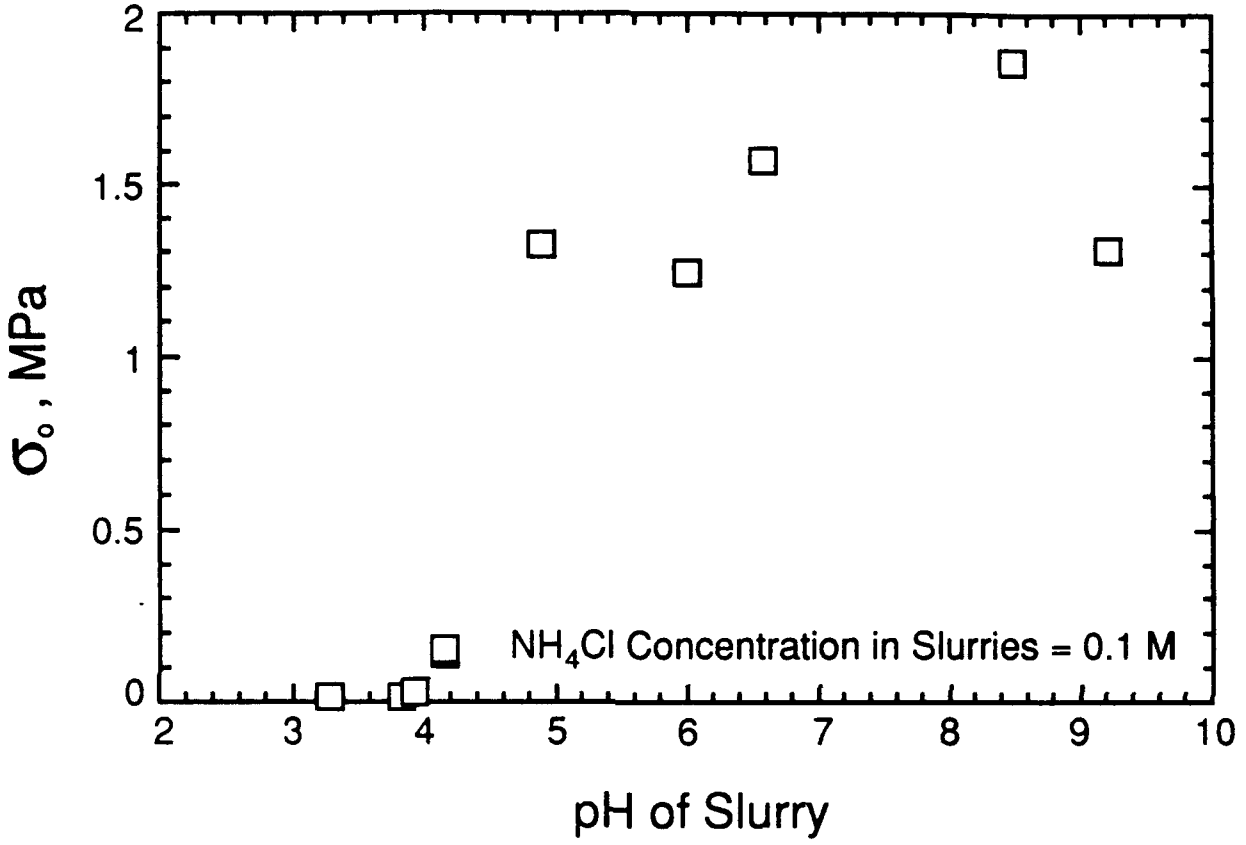

Lange.ONR-12/91-amk-D2#580-1

Velamakanni et al Fig 10

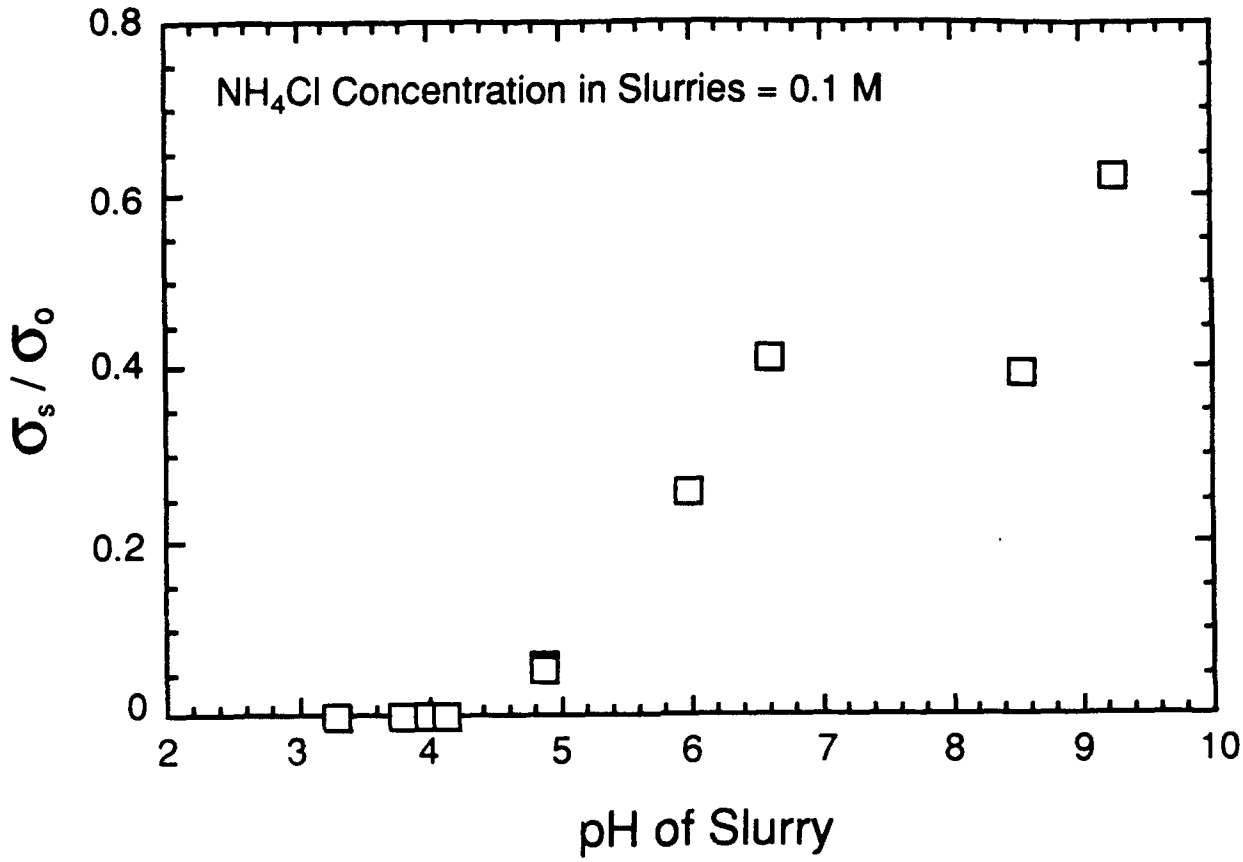

Velamakanni et al Fig 1b

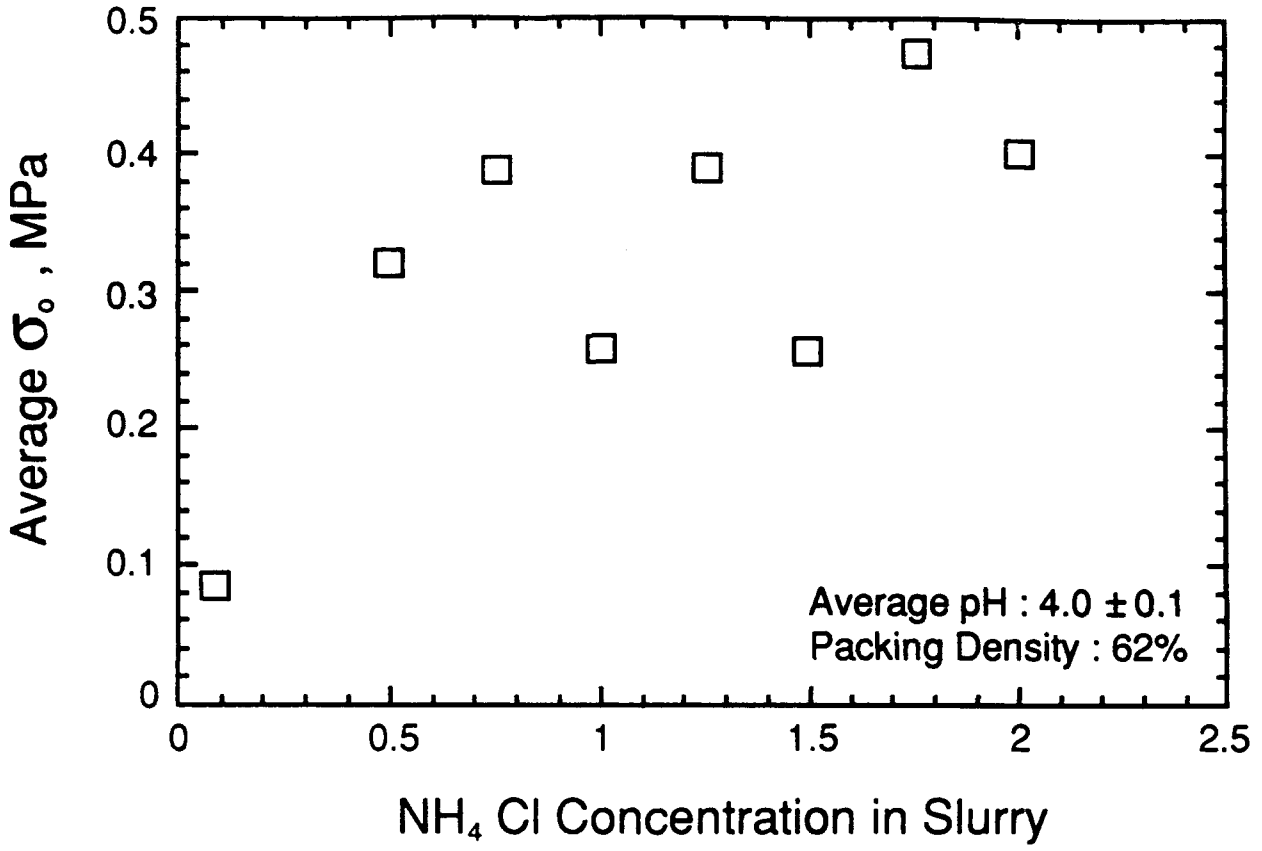

Lange.ONR-12/91-amk-D29580-3

Velamakanni et al

Fig 2

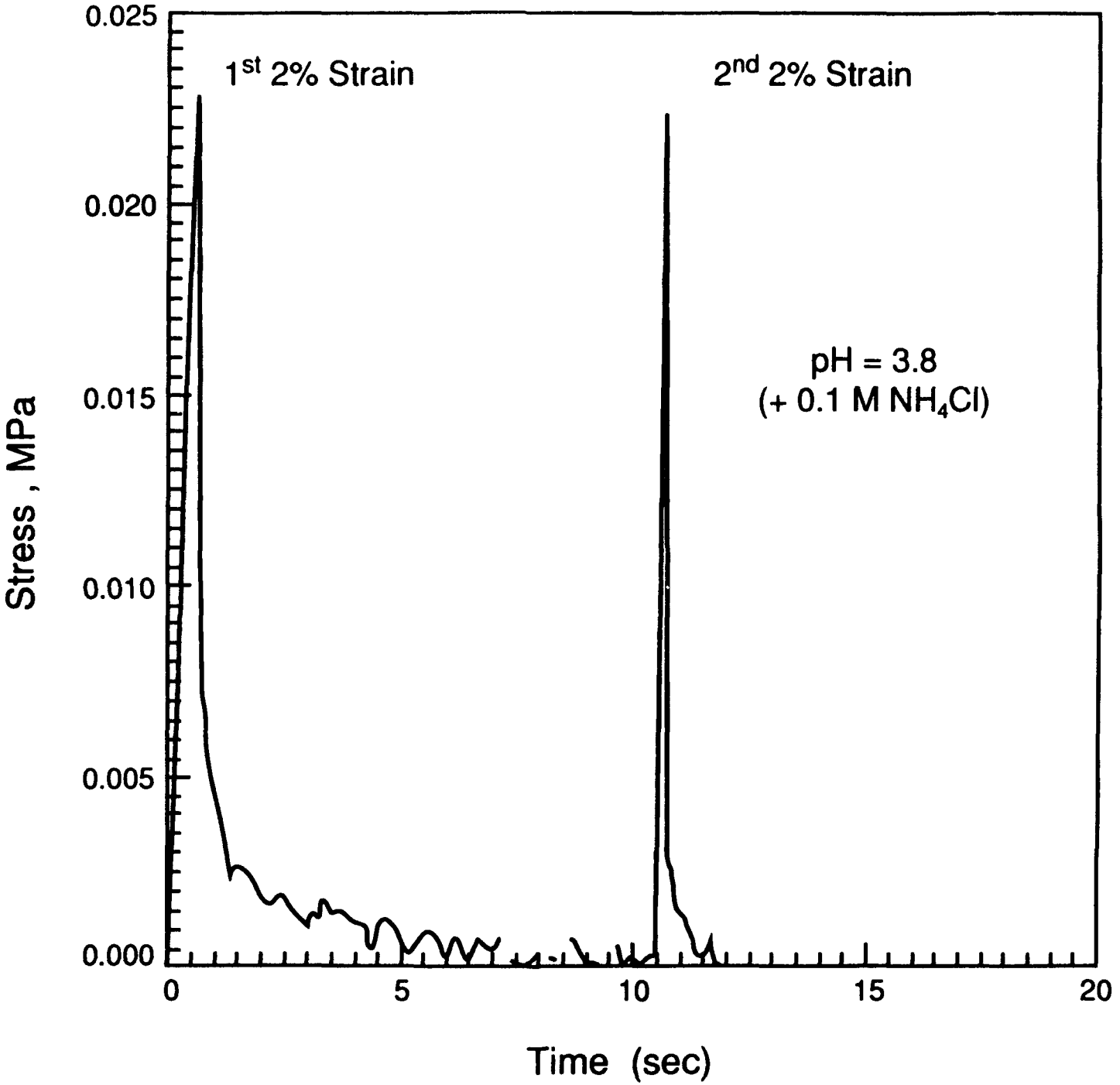

Lange ONH-12/91-amk-D2#580-4

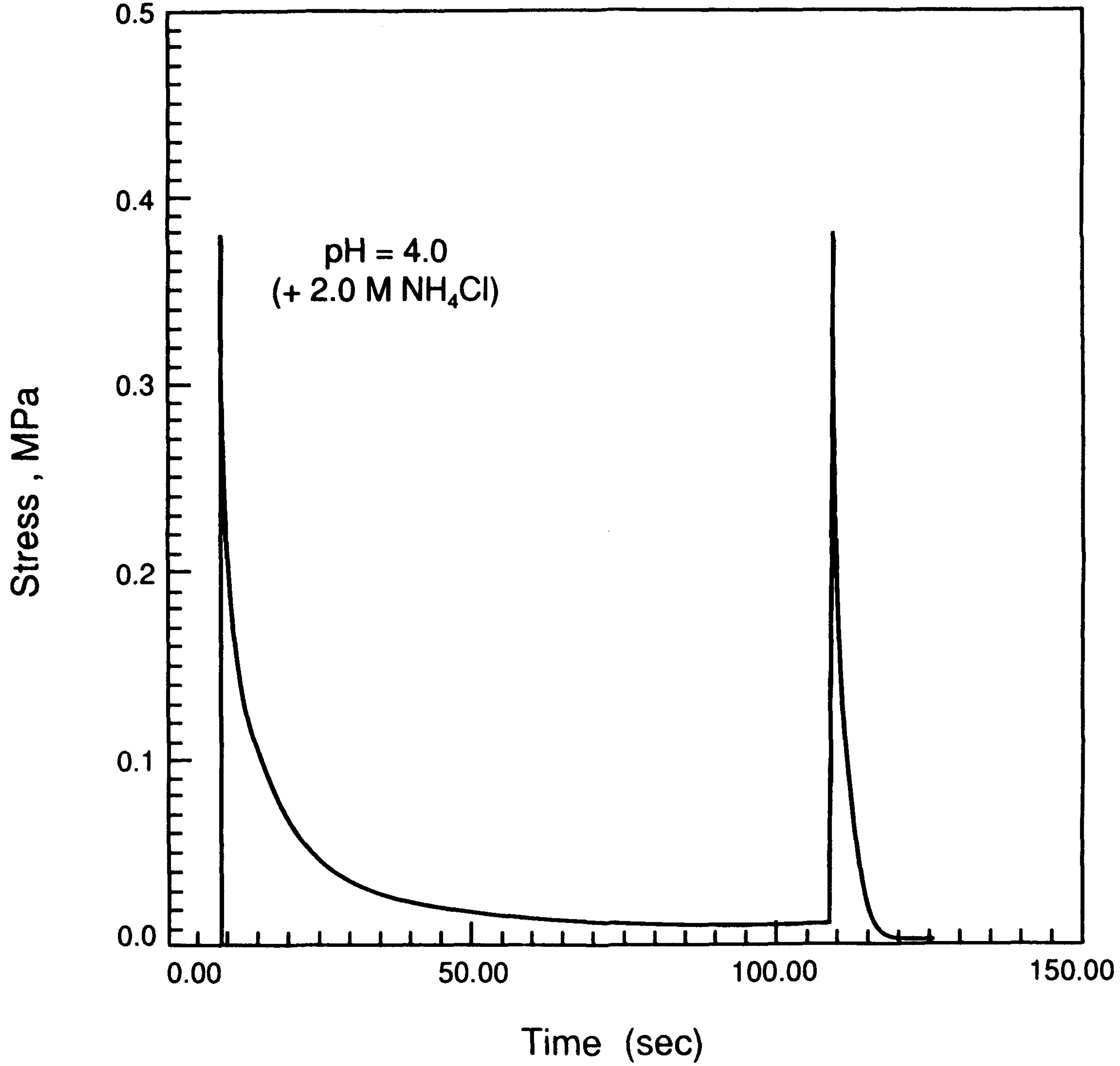
0.5
0.4
0.3
0.2
0.1
0.0
Stress , MPa
pH = 4.0
(+ 2.0 M NH4Cl)
0.00
50.00
100.00
150.00
Time (sec)

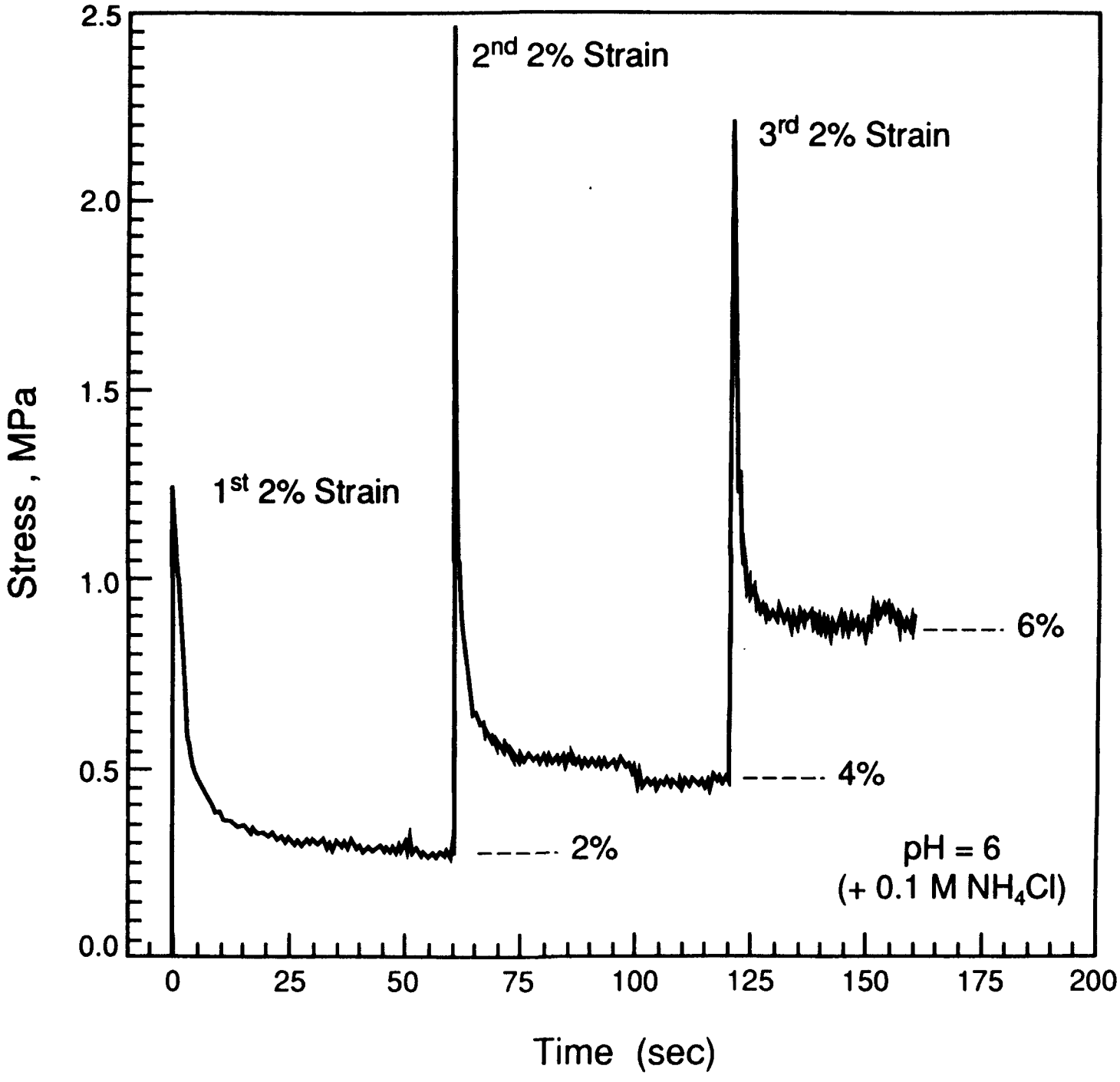
2.5
2.0
1.5
1.0
0.5
0.0
Stress , MPa
2nd 2% Strain
3rd 2% Strain
1st 2% Strain
6%
4%
2%
pH = 6
(+ 0.1 M NH4Cl)
0
25
50
75
100
125
150
175
200
Time (sec)

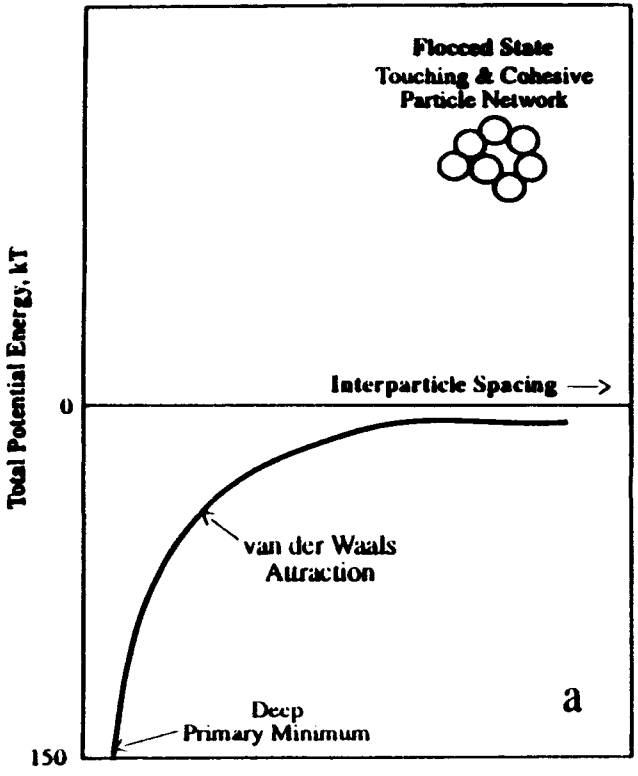
Flocced State
Touching & Cohesive
Particle Network
Interparticle Spacing →
0
Total Potential Energy, kT
van der Waals
Attraction
Deep
Primary Minimum
150
a

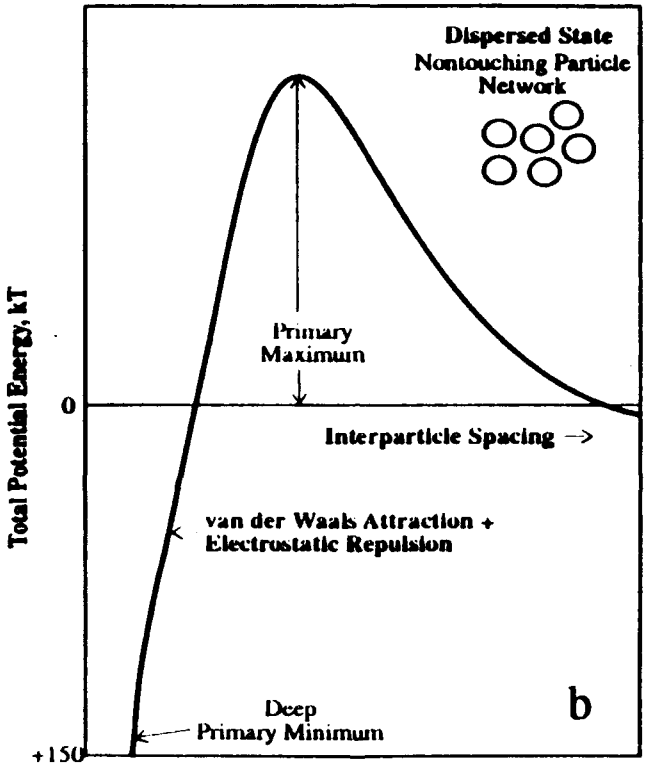
Dispersed State
Nontouching Particle
Network
Primary
Maximum
0
Interparticle Spacing →
Total Potential Energy, kT
van der Waals Attraction +
Electrostatic Repulsion
Deep
Primary Minimum
+150
b

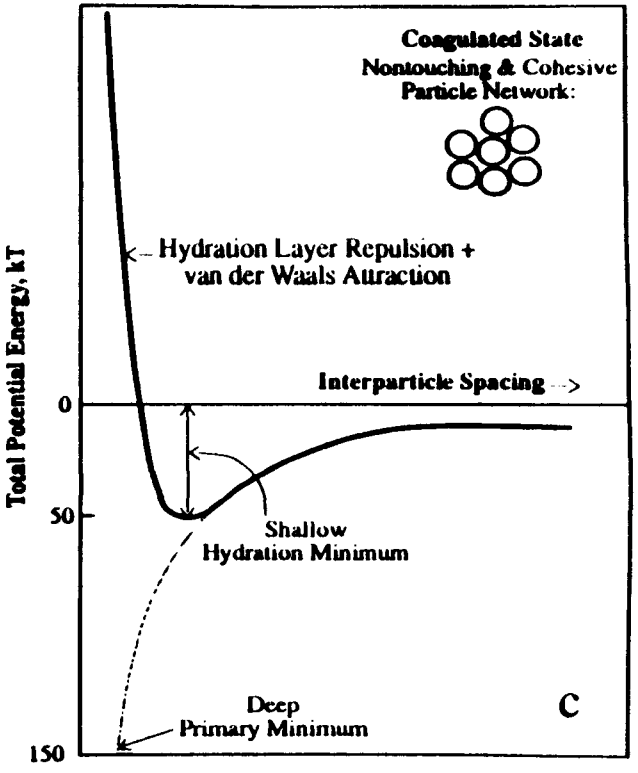
Coagulated State
Nontouching & Cohesive
Particle Network:
Hydration Layer Repulsion +
van der Waals Attraction
Interparticle Spacing →
0
Total Potential Energy, kT
50
Shallow
Hydration Minimum
Deep
Primary Minimum
150
c

MATERIALS

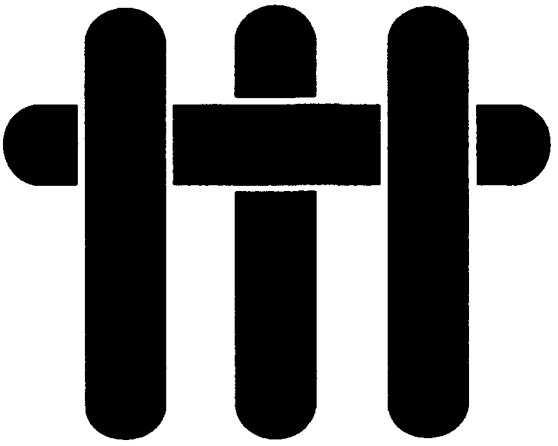

Technical Report Number 5

Enhanced Fracture Toughness in Layered Microcomposites of Ce-ZrO_2 and Al_2O_3

D. B. Marshall and J. J. Ratto
Rockwell International Science Center
and
F. F. Lange
University of California, Santa Barbara

Office of Naval Research

Grant No. N00014-90-J-1441

Fred F. Lange and Dale S. Pearson

Principal Investigators

Materials Department
University of California
Santa Barbara, CA 93106

journal

Reprinted from the Journal of the American Ceramic Society, Vol. 74, No. 12, December 1991

J. Am. Ceram. Soc., 74 [12] 2979–87 (1991)

Enhanced Fracture Toughness in Layered Microcomposites of Ce-ZrO_2 and Al_2O_3

David B. Marshall* and Joseph J. Ratto

Rockwell International Science Center, Thousand Oaks, California 91360

Fred F. Lange*

Materials Department, University of California, Santa Barbara, California 93106

Laminar composites, containing layers of Ce-ZrO_2 and either Al_2O_3 or a mixture of Al_2O_3 and Ce-ZrO_2, have been fabricated using a colloidal method that allowed formation of layers with thicknesses as small as 10 μm. Strong interactions between these layers and the martensitic transformation zones surrounding cracks and indentations have been observed. In both cases, the transformation zones spread along the region adjacent to the layer, resulting in an increased fracture toughness. The enhanced fracture toughness was observed for cracks growing parallel to the layers as well as for those that were oriented normal to the layers. [Key words: laminates, fracture toughness, cerium, zirconia, alumina.]

I. Introduction

High fracture toughnesses, in the range 10 to 14 MPa·$m^{1/2}$, have been achieved recently in ceria-partially-stabilized zirconia (Ce-TZP) that undergoes martensitic transformation from tetragonal to monoclinic phase.[1–8] However, the shapes of the transformation zones surrounding cracks in these materials are not optimal for producing large transformation toughening.[9] Whereas in other zirconia ceramics of comparable toughness (magnesia-partially-stabilized zirconia, Mg-PSZ) the transformation zone extends approximately equal distances ahead and to the side of a crack,[10] the zone in Ce-TZP is very elongated, extending ahead of the crack a distance of 10 to 20 times the zone width.[1–4] The extra transformed material ahead of the crack degrades the toughness; calculation of the crack tip shielding from zones with such shapes indicates that the increase in fracture toughness due to transformation shielding is about a factor of 2 smaller for an elongated frontal zone typical of Ce-TZP than for a semicircular frontal zone shape characteristic of Mg-PSZ.[9] Therefore, substantial benefit should result if the microstructure of Ce-TZP could be modified to change the shape of the transformation zone.

The elongated frontal zone in Ce-TZP is thought to result from autocatalytic transformation, i.e., the sequential triggering of transformation in a grain by transformation strains in adjacent grains.[5] Autocatalytic transformation also occurs in Mg-PSZ, as evidenced by the formation of well-defined shear bands within grains.[11] The microstructure of Mg-PSZ may be thought of as dual scale: the individual precipitates that transform from tetragonal to monoclinic phase are lenticular in shape (~300 nm in diameter) and are contained within grains that are larger by about 2 orders of magnitude (~50 μm in diameter).[12] Although each transformation band contains many autocatalytically transformed precipitates, the grain boundaries are effective as barriers, which arrest the propagating band. In Ce-TZP, there is no such large-scale barrier to arrest a developing transformation band; in this case, the transforming units are the individual grains and there is no larger-scale microstructural unit.

In this paper, we describe an approach for introducing a large-scale microstructural unit into Ce-TZP, in the form of layers of either Al_2O_3 or a mixture of Al_2O_3 and Ce-TZP. Based on the above discussion, the optimum separation of the layers would be expected to be a factor of ~10 to 100 times the grain size (which is ~2 μm), with individual layer thicknesses being at the lower end of the range. Layered structures satisfying this requirement have been fabricated using a colloidal method to consolidate powders. This approach has allowed formation of layers as thin as ~10 μm. Controlled crack growth experiments and indentation experiments are used to investigate the influence of these barrier layers on crack tip transformation zones and fracture toughness. The presence of the barrier layers leads to large increases in toughness and extensive *R*-curve behavior.

II. Composite Fabrication

Composites of Ce-TZP with layers of either Al_2O_3 or a mixture of 50% by volume of Al_2O_3 and Ce-ZrO_2 were fabricated using a colloidal technique. The technique involved sequential centrifuging of solutions containing suspended particles to form the layered green body, followed by drying and sintering at 1600°C for 3 h. Use was made of a technique described recently by Velamakanni *et al.*,[13] and Chang *et al.*,[14] in which an aqueous electrolyte (NH_4NO_3) was used to produce short-range repulsive hydration forces and to reduce the magnitudes of the longer-range electrostatic forces between the suspended particles. Such conditions produce a weakly attractive network of particles which prevents mass segregation during centrifugation, but, because of the lubricating action of the short-range repulsive forces, allows the particles to pack to high green density.

The relative green densities of the Al_2O_3 and Ce-ZrO_2 powders (Al_2O_3 powder from Sumitomo, Type AKP-30; Ce-ZrO_2 powder from Tosoh, Tokyo, grade TZ-12Ce) consolidated separately in this manner were approximately 60 and 50 vol%, respectively. The larger shrinkage of the Ce-ZrO_2 during subsequent sintering caused cracking in some layered composites that contained pure Al_2O_3 layers (the exceptions being some thin layers, <30 μm thick). This mismatch was minimized by using the mixed composition of 50 vol% Al_2O_3 and Ce-ZrO_2 instead of pure Al_2O_3 for most specimens.

I-W. Chen—contributing editor

Manuscript No. 196697. Received May 20, 1991; approved September 26, 1991.

Supported by the U.S. Air Force Office of Scientific Research under Contract No. F49620-89-C-0031. The colloidal science research on short-range repulsive potentials that led to the method for forming the layered structure was supported at the University of California, Santa Barbara, by the Office of Naval Research under Contract No. N00014-90-J-1141.

*Member, American Ceramic Society.

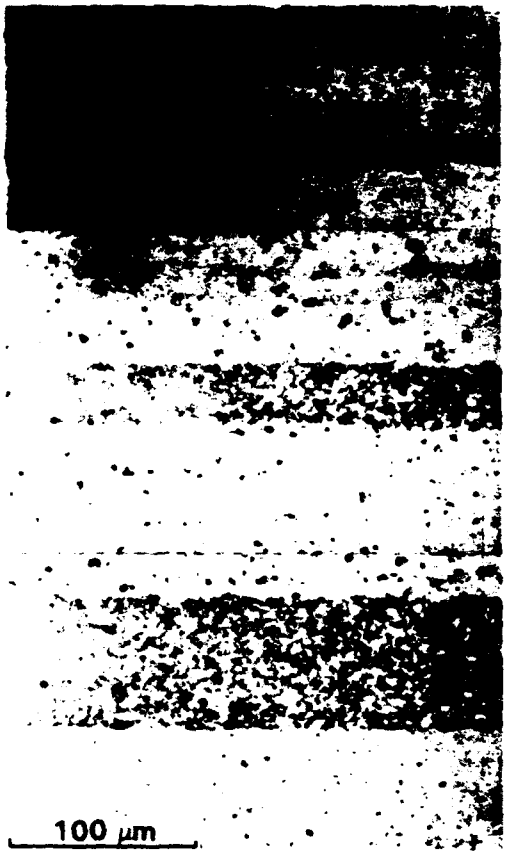

Fig. 1. Optical micrographs showing isolated layers of Al_2O_3/Ce-ZrO_2 (darker regions) with thicknesses of approximately 10, 35, and 70 μm in a matrix of Ce-TZP.

Optical micrographs of typical layers of Al_2O_3/Ce-ZrO_2 within a matrix of Ce-TZP are shown in Fig. 1. Reasonably uniform layers with thicknesses in the range 10 to 100 μm were readily formed. A multilayered structure of alternating Ce-TZP and Al_2O_3/Ce-ZrO_2 layers of thickness 35 μm is shown in Fig. 7.

III. Mechanical Properties

(1) The Role of Isolated Layers

The influence of individual layers of Al_2O_3 or 50% Al_2O_3/Ce-ZrO_2 on crack growth and transformation zones in Ce-TZP was investigated by fabricating composites containing widely spaced layers. Measurements were obtained from controlled crack growth in notched beams, fracture of smooth bars, and indentation experiments using a Vickers indenter.

Crack growth experiments with notched beams were done in two steps, using two different loading fixtures, which operated on the stage of an optical microscope and allowed high-magnification observation of the side of the beam during loading. All experiments were done in a dry nitrogen atmosphere. The dimensions of the beams were approximately 28 mm × 6 mm × 1 mm, with the initial notch of 170-μm width and approximately 2-mm depth. First, a stable crack was initiated from the root of the notch under monotonic loading, using the fixture illustrated in Fig. 2(a). The WC/Co flexure beams in series with the test specimen make the loading system extremely stiff and thereby allow stable crack growth. The beams are equivalent to very stiff springs in *parallel* with the specimen and thus act as a crack arrester, as described for different geometrical arrangements by Mai and Atkins[15] and Sakai and Inagaki.[16] This initial crack growth was induced without use of a load cell, in order to stiffen the loading system further. After thus growing the crack for ~500 μm, the loading system was changed to include a load cell with conventional four-point loading through rollers (Fig. 2(b)) in order to allow measurement of the fracture toughness (or crack growth resistance). The stress intensity factor was evaluated from the measured loads and crack lengths (obtained from optical micrographs) using the expression from Ref. 17.

Results that were obtained from a specimen containing three layers of Al_2O_3–Ce-ZrO_2 widely spaced ahead of the notch are shown in Fig. 3. After initiating stably in the immediate vicinity of the notch, the crack grew unstably when the loading system was changed to include the load cell, and arrested approximately 20 μm before the first layer of Al_2O_3/ZrO_2 (which had a thickness of ~35 μm). The width of the transformation zone over the wake of the crack, as determined by Nomarski interference, was approximately 15 μm. However, near the tip of the arrested crack, the transformation zone extended adjacent to the Al_2O_3/ZrO_2 layer for distances of more than 150 μm each side of the crack, as shown schematically in Fig. 3(b). Some transformation also occurred on the opposite side of the Al_2O_3/ZrO_2 layer, also for a distance of 150 μm both sides of the crack plane.

After further loading, the crack grew unstably through the Al_2O_3/ZrO_2 layer, into the Ce-TZP on the opposite side, and arrested again ~40 μm before the second layer (which had a thickness of 70 μm). The shape of the transformation zone

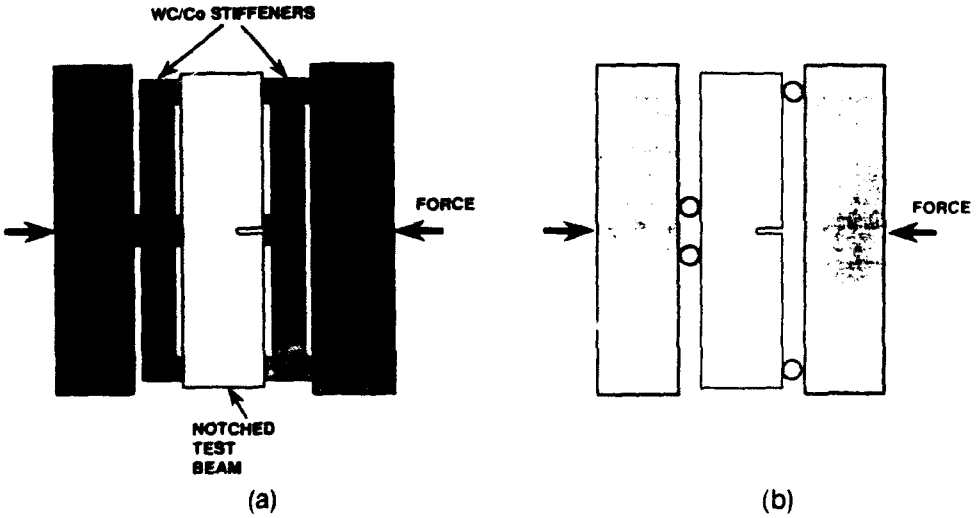

Fig. 2. Loading fixtures for notched beam fracture testing: (a) high-stiffness system used for crack initiation; (b) conventional system used for stress intensity factor measurements.

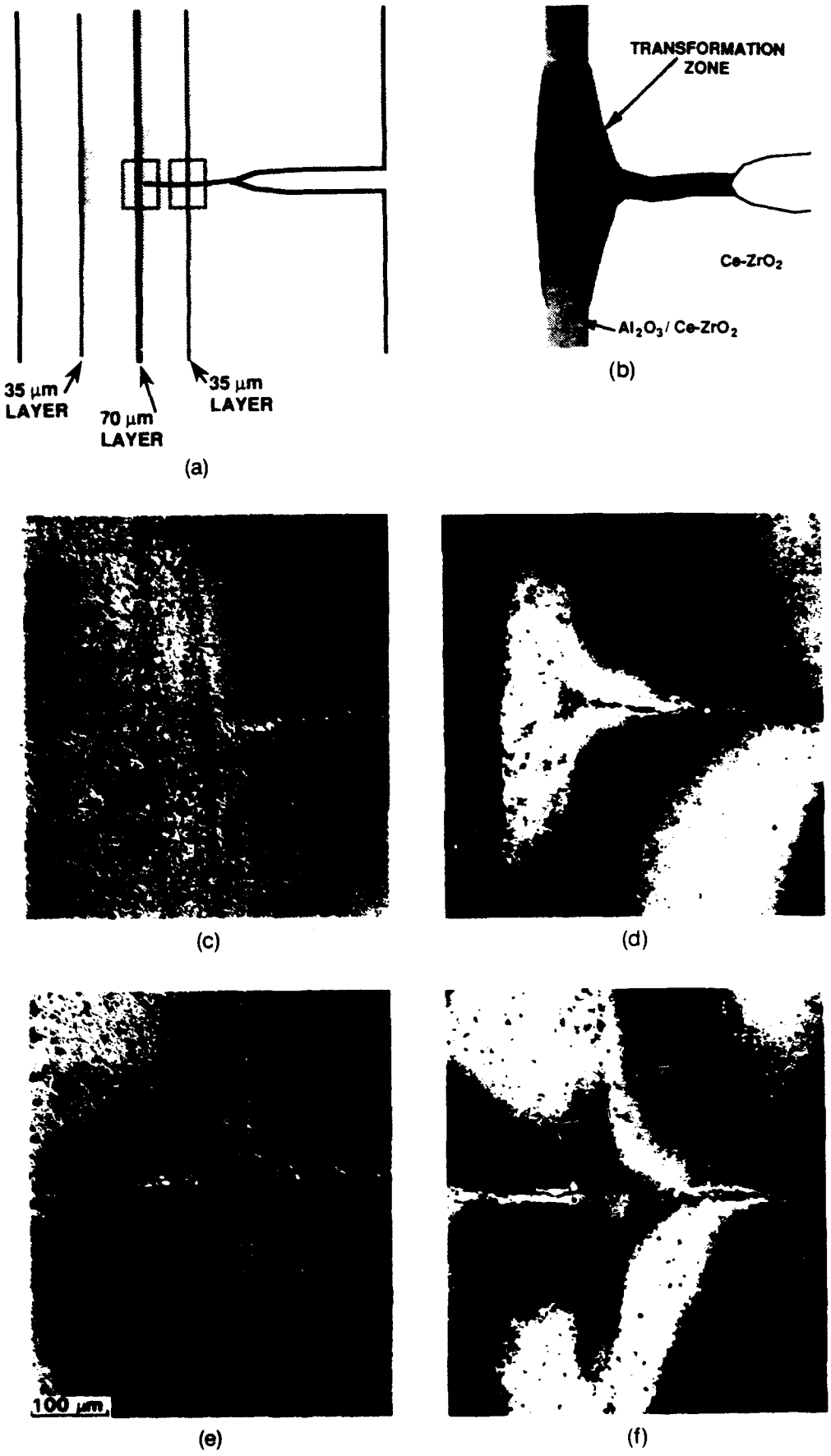

Fig. 3. Schematic of notched beam of Ce-TZP containing three layers of $Al_2O_3/Ce\text{-}ZrO_2$. (b) Schematic diagram of arrested crack near $Al_2O_3/Ce\text{-}ZrO_2$ layer, showing shape of enlarged transformation zone adjacent to the layer. (c) Nomarski interference micrograph showing arrested crack tip near Al_2O_3/ZrO_2 layer (area indicated in (a)) with widened transformation zone adjacent to layer. (d) Two-beam interference micrograph of area in (b). Reference mirror is parallel to surface remote from crack, so that fringes represent contours of constant surface uplift (due to transformation strains). (e, f) Micrographs taken as in (c) and (d) from the region in the crack wake near the first Al_2O_3/ZrO_2 layer, as indicated in (a).

along the layer near the crack tip was similar to that at the first arrest position. Nomarski interference and two-beam interference micrographs of regions around the first and second layers, with the crack tip at this position, are shown in Figs. 3(c) to (f). These results indicate that the Al_2O_3/ZrO_2 barrier layers have a much larger effect than simply arresting the growth of a transformation zone ahead of a crack; they also promote expansion of the zone to the side of the crack, which is the location that gives rise to crack tip shielding and hence toughening.[18–20]

The applied stress intensity factors were calculated at various stages of crack growth, using the measured loads and crack lengths. The fracture toughness of the Ce-ZrO_2 matrix was ≈ 5 MPa $\cdot$ m$^{1/2}$, whereas the stress intensity factor had to be raised to ≈ 10 MPa $\cdot$ m$^{1/2}$ to drive the crack across each layer. After the crack tip passed each layer, the unstable crack growth prevented continued measurement of the stress intensity factor until the crack arrested again. However, when the crack had arrested the applied stress intensity factor had decreased to ~ 5 MPa $\cdot$ m$^{1/2}$, indicating that the toughening effect of each layer decreased as it moved further into the wake of the crack. Similar results were obtained from specimens containing layers of 100% Al_2O_3 in the same Ce-TZP matrix.

Smooth beams of the same composite as in Fig. 3 were broken in bending in the two orientations shown in Figs. 4(a) and (b). In the orientation of Fig. 4(a), which is the same as that of the notched beam, failure occurred unstably at a critical load. The polished side surfaces of the beams exhibited similar evidence for widening of the transformation zone near the Al_2O_3/ZrO_2 layers as in Figs. 3(b) to (f). Therefore, this beneficial interaction occurs for fast-moving as well as stable cracks. In the orientation of Fig. 4(b), fracture also initiated unstably from the tensile surface at a critical load. However, the crack arrested before it reached the opposite side, leaving the beam intact (Fig. 4(c)). The effectiveness of the Al_2O_3/ZrO_2 layers in arresting this crack is especially noteworthy since there were only two layers in the beam, accounting for 2% of its volume. On the surface that had been loaded in tension, there were several narrow bands of transformed material in addition to the crack that caused the sudden load drop, similar to observations in the literature.[2,5,6] However, some of the transformation bands were arrested at the Al_2O_3/ZrO_2 layers. There is also evidence that the crack itself arrested at the Al_2O_3/ZrO_2 layer before joining with a second crack to cause failure.

Vickers indentations in the Ce-TZP were surrounded by large zones of transformed material, which caused uplift of the surface adjacent to the indentations. Micrographs, obtained using both Nomarski interference and two-beam interference, of several such zones in the vicinities of Al_2O_3/ZrO_2 layers are shown in Fig. 5. At indentation loads up to 300 N, there was no cracking caused by the indentations. The presence of a nearby Al_2O_3/ZrO_2 layer within the transformation zone caused spreading of the zone in the region adjacent to the layer, in a pattern that is similar to the crack tip zone spreading of Fig. 3. There was also transformed material on the side opposite the indentation. The surface uplift, measured from the optical interference micrograph of Fig. 5(b), is plotted in

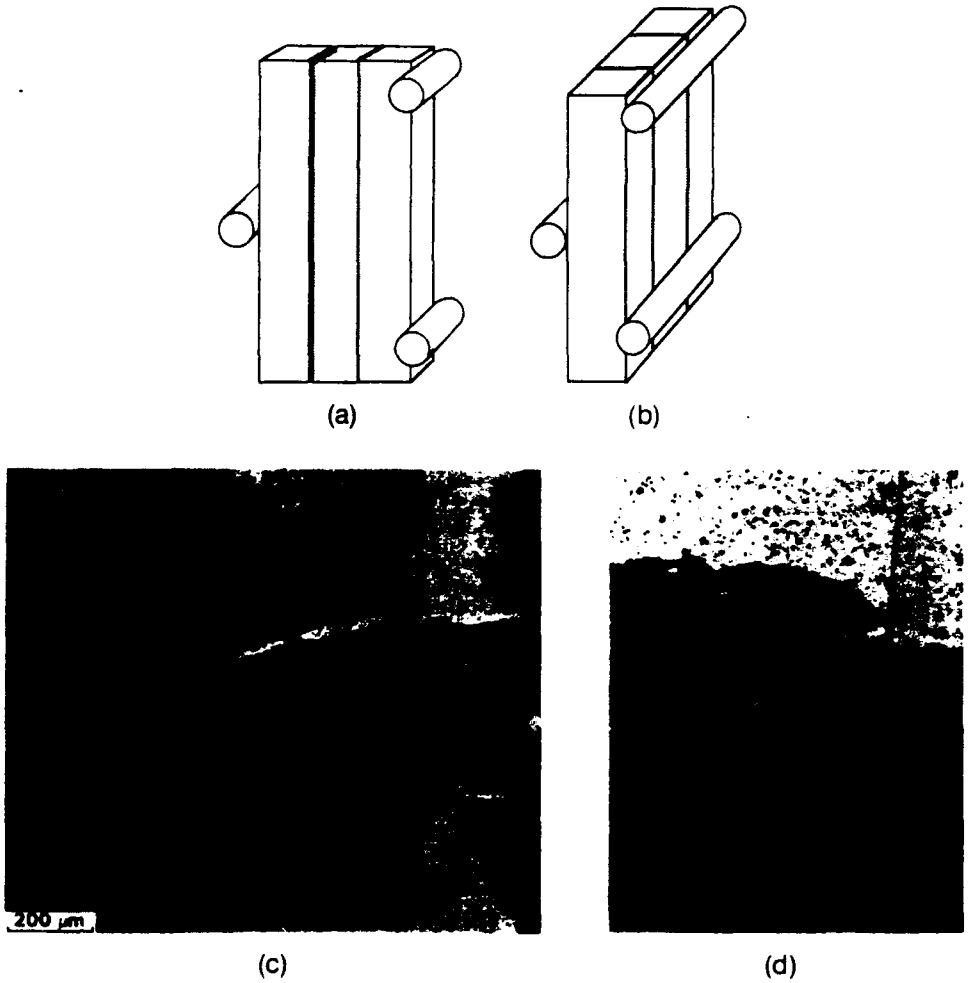

Fig. 4. (a, b) Bending test geometry showing orientations of Al_2O_3/ZrO_2 layers relative to bending direction. (c) Side view of crack in specimen oriented as in (b), showing crack arrest before complete failure. (d) Tensile surface of specimen from (c) showing crack arrest at Al_2O_3/ZrO_2 layer and arrest of transformation bands at the Al_2O_3/ZrO_2 layer (note the transformation band can also be seen on the side surface in (c)).

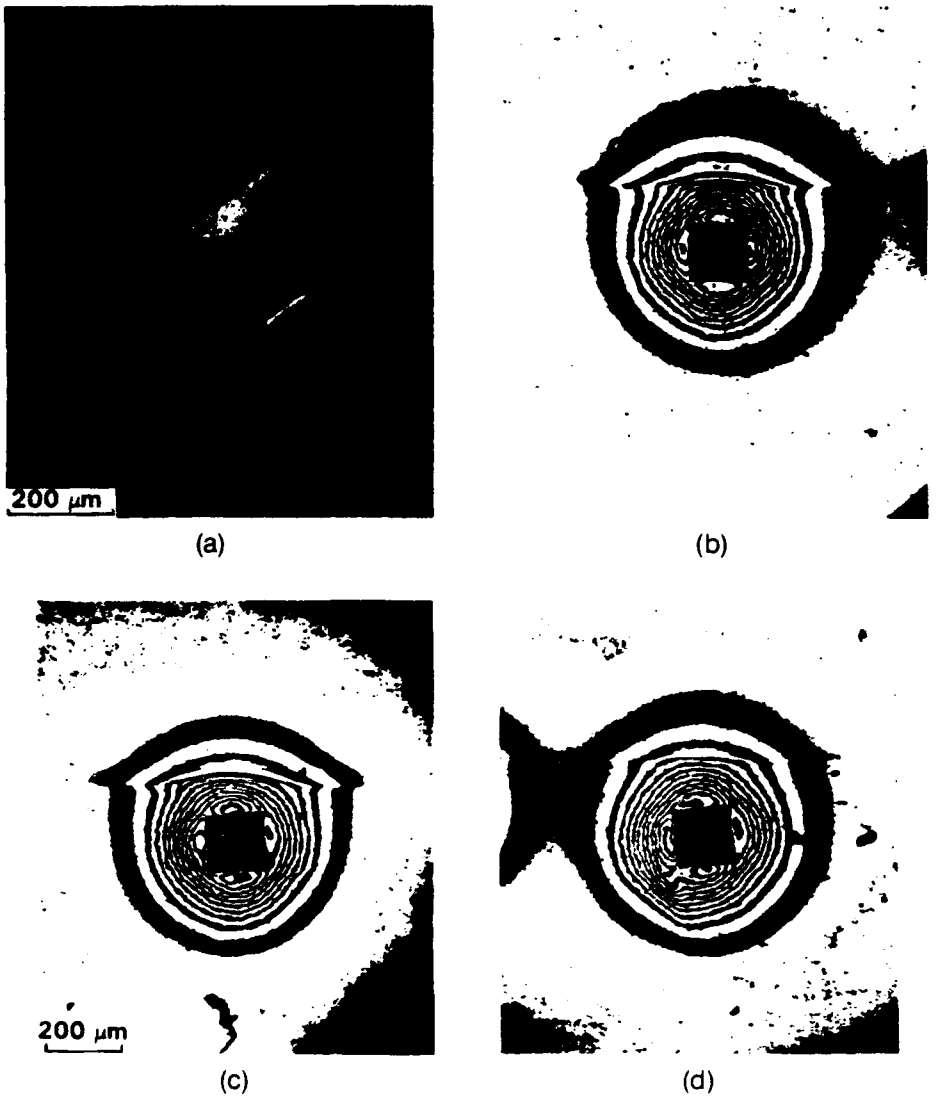

Fig. 5. Vickers indentation (200-N load) near layers of Al_2O_3 and Al_2O_3/ZrO_2 showing interaction of layers with transformation zone. (a) Nomarski interference, Al_2O_3/ZrO_2 layer 30 μm thick. (b–d) Optical interference micrographs with reference mirror parallel to specimen surface remote from indentations (fringes represent contours of surface uplift): (b) Al_2O_3/ZrO_2 layer 30 μm thick, (c) Al_2O_3 layer 30 μm thick, and (d) Al_2O_3 layer 10 μm thick.

Fig. 6 along several lines near the indentation, as depicted in the inset of Fig. 6. The presence of the Al_2O_3/ZrO_2 layer caused substantially larger uplift everywhere on the side of the indentation that is closer to the layer. The surface of the Al_2O_3/ZrO_2 layer is depressed relative to the adjacent transformed Ce-TZP material. However, this Al_2O_3/ZrO_2 layer is uplifted *more* than the Ce-TZP surface at corresponding positions on the opposite side of the indentation. This observation provides evidence that the Al_2O_3/ZrO_2 layer caused spreading of the transformation zone adjacent to the layer in the subsurface regions as well as along the surface, and/or a larger concentration of transformed material in the region adjacent to the layer.

(2) Response of Multilayered Structures

The influence of multilayered microstructures on transformation zone shapes and toughening was investigated using a specimen containing 19 layers of alternating Ce-TZP and Al_2O_3/ZrO_2, each of 35-μm thickness, in the center of a beam of Ce-TZP. An additional isolated 35-μm layer of Al_2O_3 was located ~1 mm from the multilayered region (Fig. 7(a)).

The toughening experienced by cracks oriented normal to the layers was evaluated by growing a crack in a notched beam using the loading procedure described in the previous section. The tip of the initial crack that was introduced with the stiff loading system was about halfway between the end of the notch and the first of the multiple layers (550 μm from the notch and 440 μm from the first layer). Further loading with the more compliant loading system, which allowed continuous load measurement, caused stable growth up to and

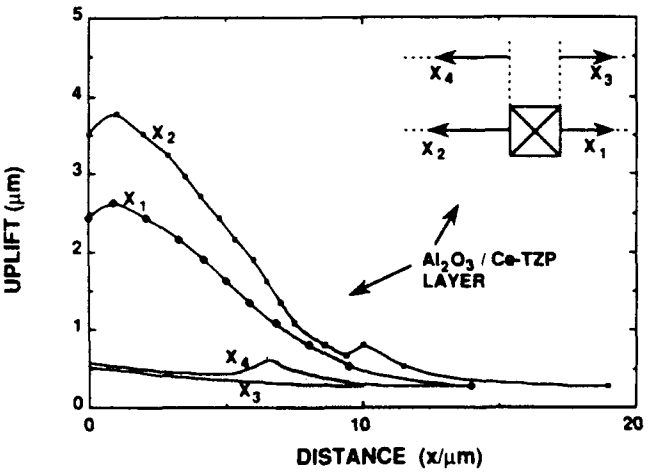

Fig. 6. Surface uplift measured from Fig. 5(b) along four paths as indicated.

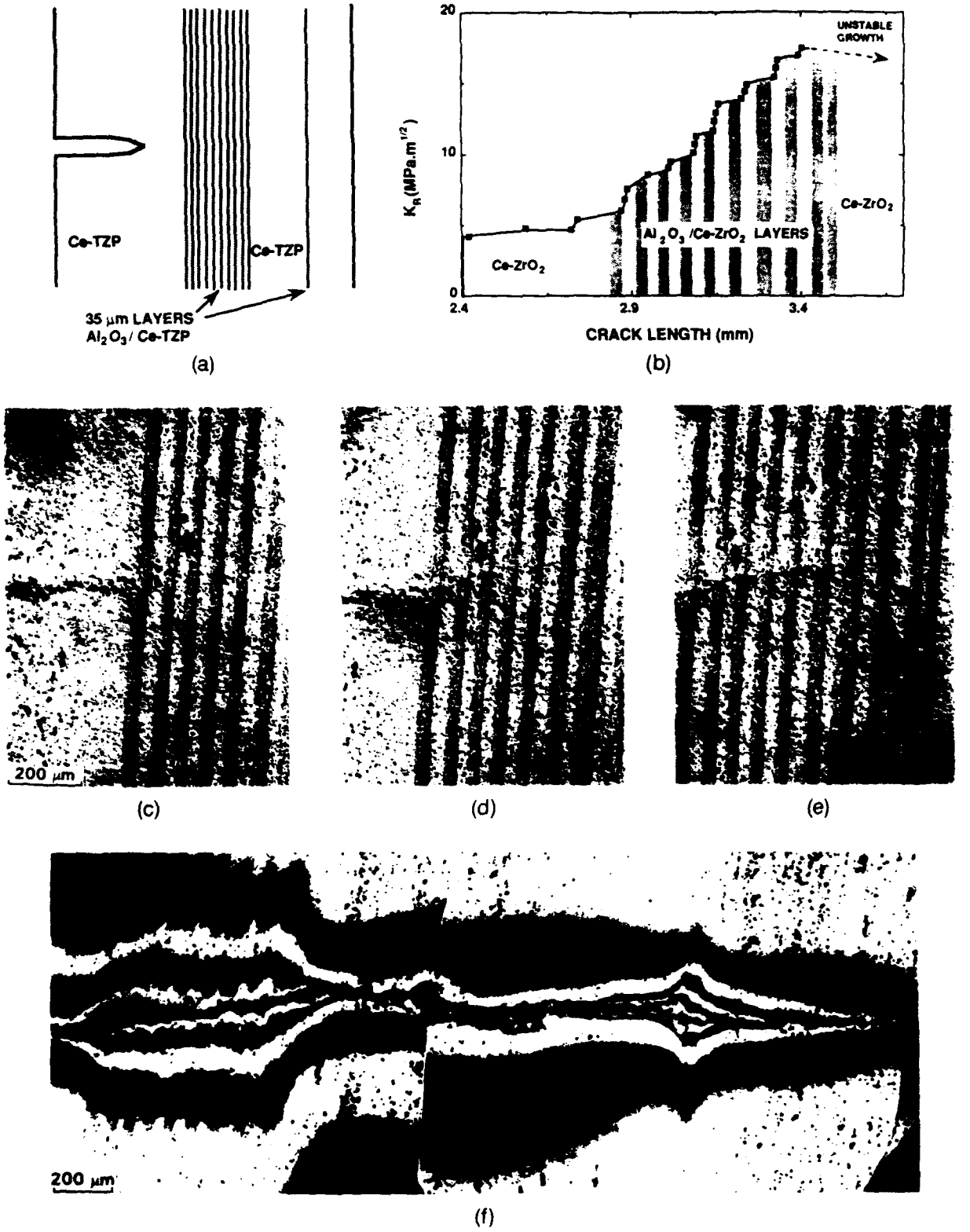

Fig. 7. (a) Multilayered region embedded within a matrix of Ce-TZP. (b) Critical applied stress intensity factor for crack growth up to and through the multilayered region of (a). (c–e) In situ optical micrographs (Nomarski interference) showing crack tip at several stages of growth through the multilayered region. (f) Optical interference micrographs of specimen in (a) to (c) after the crack had grown past the isolated layer. Reference mirror is parallel to undistorted specimen surface, so that fringes represent contours of out-of-plane surface displacements (the discontinuity in the lower central region is due to the joining of two micrographs with imperfect matching of the reference mirror positions).

through the multiple layers. However, as the crack approached the last of the layers, it extended unstably for 1.5 mm and arrested at a position 400 μm past the isolated layer.

The applied stress intensity factor, K_R, needed to extend the crack up to and through the multiple layers is shown in Fig. 7(b), and micrographs showing the crack tip at several positions within the layers are shown in Figs. 7(c) to (e). The critical stress intensity factor increased from approximately 5 MPa · m$^{1/2}$ in the Ce-TZP to 17.5 MPa · m$^{1/2}$ as the crack approached the end of the layered region. A corresponding increase in the size of the transformation zone surrounding the crack tip is evident in the micrographs of Figs. 7(c) to (e).

Surface distortions due to the volume strain associated with the transformation can be detected as far as 300 μm from the crack plane, whereas the zone width in the single phase Ce-TZP is only ~15 μm.

The increased width of the transformation zone within the layered region is more clearly evident in the optical interference micrograph of Fig. 7(f), in which the fringes represent contours of surface uplift adjacent to the crack. This micrograph was obtained after the load was removed at the conclusion of the experiment. The surface uplift adjacent to the crack is also larger (by a factor of about 2) within the layered region than in the single-phase Ce-TZP, even though the uplift is constrained by the higher-stiffness Al_2O_3/ZrO_2 layers, and the average volume fraction of the $Ce\text{-}ZrO_2$ is lower in the layered region. Both the zone width and the magnitude of the surface uplift adjacent to the crack decreased where the crack grew unstably out of the multilayered region into the single-phase $Ce\text{-}ZrO_2$, and increased again as the crack passed through the isolated Al_2O_3/ZrO_2 layer.

The response of cracks oriented parallel to the layers was assessed by loading a double cantilever beam using another fixture on the stage of the optical microscope. The cantilever beam was cut, as shown in Fig. 8(a), from a region of the specimen that contained a conveniently located large processing flaw, which served as an initial sharp crack (a flat nonsintered region ~1 mm in diameter at the edge of the multilayered area). Micrographs obtained at two stages during loading are shown in Figs. 8(b) and (c). As the load was increased initially, a zone of material within the single-phase Ce-TZP ahead and to one side of the crack tip transformed before the crack began to grow. With further load increase, the crack grew but was forced to cross the first layer of Al_2O_3/ZrO_2, presumably because of the compressive stresses due to the transformation zone on one side of the crack. The crack then grew along the first layer of $Ce\text{-}ZrO_2$ within the multilayered region, causing transformation in an increasingly wide zone of adjacent layers. The stress intensity factor was not evaluated during this test because the ends of the beam were glued into the loading fixture rather than being loaded through pins. Nevertheless, it is clear that the layers caused an enhancement of the width of the transformation zone, and hence the toughness, in this orientation as well as in the normal orientation.

IV. Discussion

The results in the previous section show that the presence of layers of Al_2O_3 or Al_2O_3/ZrO_2 in Ce-TZP can dramatically modify the sizes and shapes of the transformation zones around cracks. Two effects have been identified. One is the anticipated truncation of the elongated frontal zone, as discussed in the Introduction, which can increase the toughening due to crack shielding by a factor of approximately 2. The other, unexpected effect is the spreading of the transformation zones along the regions adjacent to the layers.

The zone spreading must be driven by the modification of the stress field outside the transformation zone resulting from the nontransformable nature of the layers and/or their higher elastic stiffness. Residual stress due to the difference in thermal expansion coefficients of the Ce-TZP and the Al_2O_3-containing layers could potentially influence zone spreading in multilayered composites, where, for example, the magnitude of the stress would be as high as ~100 MPa if the layer thicknesses were equal. However, in the present experiments, the zone spreading was observed around cracks and indentations near isolated layers, which represented less than 1% of the total specimen volume. In this case the residual stress in the Ce-TZP was negligibly small and therefore was not a significant influence on the spreading of the transformation zones. This conclusion is further supported by observations that layers containing 50% Al_2O_3 or 100% Al_2O_3 (for which the thermal expansion mismatches with the Ce-TZP differ) caused the same degree of zone spreading (e.g., Figs. 5(b) and (c)).

The combined effects of the zone spreading and truncation caused an increase in the fracture toughness of the layered material by a factor of 3.5 (from 5 to 17.5 MPa·$m^{1/2}$). Noting that the measured toughnesses are given by the sum of the

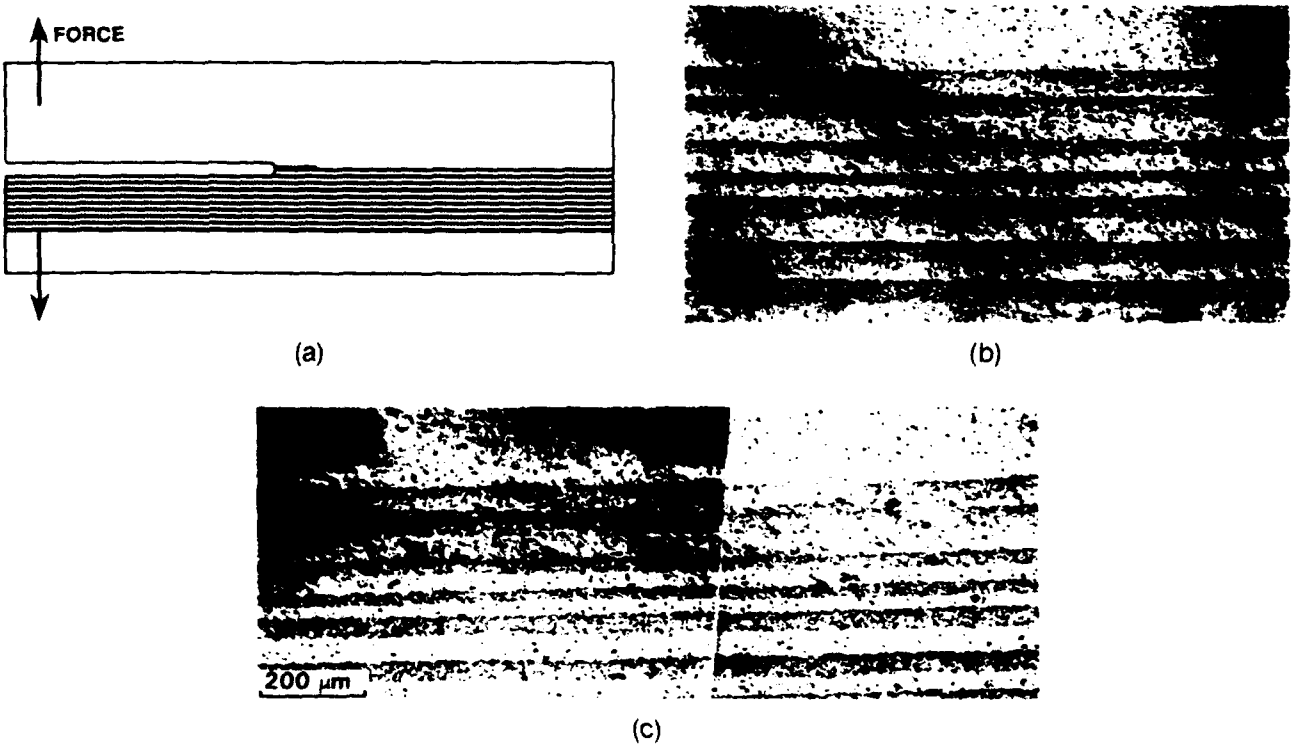

Fig. 8. (a) Schematic diagram of double cantilever beam cut from same composite as in Fig. 7. (b, c) In situ optical micrographs (Nomarski interference) showing crack and surrounding transformation zone at several stages of growth along the layers.

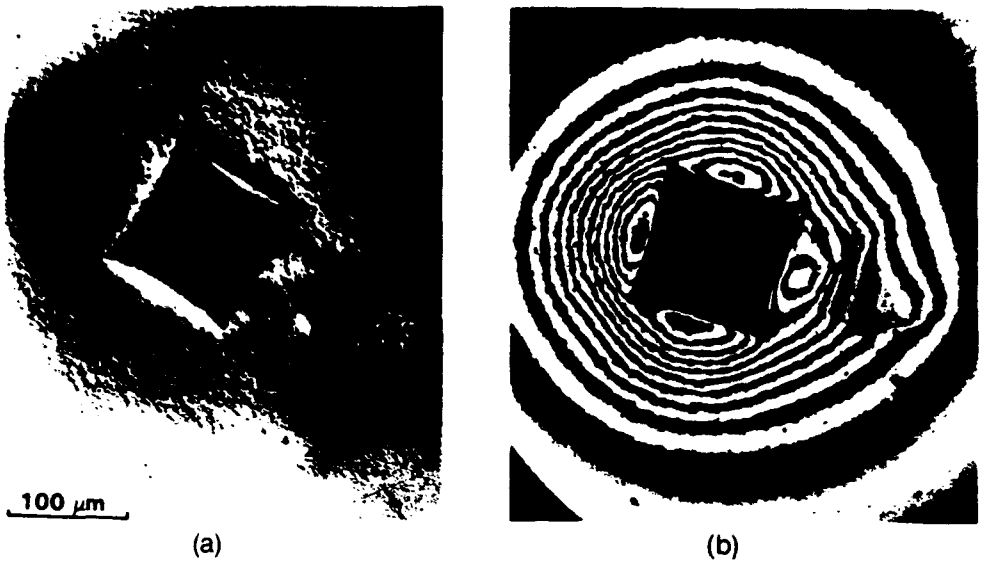

Fig. 9. Vickers indentation (200-N load) near sapphire fiber in Ce-TZP matrix, showing interaction of fiber with transformation zone: (a) Nomarski interference, (b) two-beam interference with reference mirror parallel to specimen surface remote from indentation.

intrinsic toughness of the Ce-TZP without any transformation zone and the crack tip shielding component, K_s, due to the transformation zone, the observed toughness increase corresponds to an increase in K_s by a factor of 5.

The Ce-ZrO_2 material used in this preliminary study exhibited a fracture toughness of ~5 MPa·$m^{1/2}$ and a transformation zone size of ~15 μm (Figs. 7(b) and (c)). These values are substantially smaller than the toughnesses and zone sizes reported in more transformable Ce-ZrO_2 materials[1-8] ($K_R \approx$ 14 MPa·$m^{1/2}$ and zone sizes of several hundred micrometers). However, despite this relatively low starting toughness, the multilayered microstructure was characterized by a crack resistance curve that went as high as 17.5 MPa·$m^{1/2}$, and which had not begun to saturate to a steady-state value when the crack encountered the end of the layered microstructure. This peak value of K_R is one of the highest toughnesses recorded in a ceramic material, being surpassed only by weakly bonded fiber-reinforced composites,[21] weakly bonded laminar composites,[22] and by some Mg-PSZ materials immediately after heat treatment[23,24] (the high-toughness Mg-PSZ materials age and lose some of their toughening at room temperature). There is clearly a potential for substantially higher fracture toughnesses in layered microstructures fabricated with the higher-toughness Ce-TZP starting materials. Fabrication of such materials is under way.

The mechanisms of toughening enhancement observed here should not be restricted to the laminar geometry used in this study. Similar effects may be expected for any high-modulus, nontransforming microstructural unit, such as continuous or chopped fibers or platelets, distributed over a similar spatial scale as the layers. An example of the interaction of a transformation zone around an indentation with an isolated sapphire fiber in the Ce-TZP matrix is shown in Fig. 9. By direct analogy with the effect of the Al_2O_3 layers, the sapphire fiber caused spreading of the transformation zone and a larger overall surface uplift in the vicinity of the fiber.

V. Conclusions

Laminar composites containing alternating layers of Ce-TZP and a mixture of Al_2O_3 and Ce-ZrO_2 have been fabricated using a colloidal technique. In situ observations during controlled crack growth experiments in these microcomposites have yielded the following results:

(1) The layers interacted strongly with the transformation zones surrounding cracks and indentations, causing the zones to spread along the regions adjacent to the layers and leading to enhanced fracture toughness.

(2) Multilayered microstructures exhibited *R*-curve behavior for cracks oriented normal to the layers, with the critical stress intensity factor increasing by a factor of 3.5 from the starting toughness of the Ce-TZP (~5 MPa·$m^{1/2}$) to a value of at least 17.5 MPa·$m^{1/2}$. (This peak value had not saturated to a steady state, but instead was limited by the crack having reached the end of the multilayered region.)

(3) Zone spreading and toughening effects were observed for cracks growing parallel to the layers as well as for those oriented normal to the layers.

References

[1] M.V. Swain, R. H. J. Hannink, and J. Drennan, "Some Interfacial Related Properties of Transformation Toughened Ceramics"; p. 819 in *Ceramic Microstructures '86, Role of Interfaces*. Edited by J. A. Pask and A. G. Evans. Plenum, New York, 1987.

[2] R. H. J. Hannink and M. V. Swain, "Metastability of Martensitic Transformation in a 12 mol% Ceria–Zirconia Alloy: Deformation and Fracture Observations," *J. Am. Ceram. Soc.*, **72** [1] 90–98 (1989).

[3] L. R. F. Rose and M. V. Swain, "Transformation Zone Shape in Ceria-Partially-Stabilized Zirconia," *Acta Metall.*, **36** [4] 955–62 (1988).

[4] C.-S. Yu and D. K. Shetty, "Transformation Zone Shape, Size, and Crack-Growth-Resistance (*R*-Curve) Behavior of Ceria-Partially-Stabilized Zirconia Polycrystals," *J. Am. Ceram. Soc.*, **72** [6] 921–28 (1989).

[5] P. E. Reyes-Morel and I-W. Chen, "Transformation Plasticity of CeO$_2$-Stabilized Tetragonal Zirconia Polycrystals: I. Stress Assistance and Autocatalysis," *J. Am. Ceram. Soc.*, **72** [5] 343–53 (1988).

[6] P. E. Reyes-Morel, J.-S. Cherng, and I-W. Chen, "Transformation Plasticity of CeO$_2$-Stabilized Tetragonal Zirconia Polycrystals: II. Pseudoelasticity and Shape Memory Effects," *J. Am. Ceram. Soc.*, **71** [8] 648–57 (1988).

[7] K. E. Tsukuma and M. Shimada, "Strength, Fracture Toughness, and Vickers Hardness of CeO$_2$-Stabilized Tetragonal Zirconia Polycrystals (Ce-TZP)," *J. Mater. Sci.*, **204** [4] 1178–84 (1985).

[8] T. Sato, T. Endo, and M. Shimada, "Postsintering Hot Isostatic Pressing of Ceria-Doped Tetragonal Zirconia Alumina Composites in an Argon-Oxygen Gas Atmosphere," *J. Am. Ceram. Soc.*, **72** [5] 761–64 (1989).

[9] D. B. Marshall, "Crack Shielding in Ceria-Partially-Stabilized Zirconia," *J. Am. Ceram. Soc.*, **73** [10] 3119–21 (1990).

[10] D. B. Marshall, M. C. Shaw, R. H. Dauskardt, R. O. Ritchie, M. Readey, and A. H. Heuer, "Crack Tip Transformation Zones in Toughened Zirconia," *J. Am. Ceram. Soc.*, **73** [9] 2659–66 (1990).

[11] A. H. Heuer, M. Rühle, and D. B. Marshall, "On the Thermoelastic Transformation in Tetragonal ZrO$_2$," *J. Am. Ceram. Soc.*, **73** [4] 1084–93 (1990).

[12] R. H. J. Hannink and M. V. Swain, "Magnesia-Partially-Stabilized Zirconia: The Influence of Heat Treatment on Thermomechanical Properties," *J. Aust. Ceram. Soc.*, **18** [2] 53–62 (1982).

[13] B. V. Velamakanni, J. C. Chang, F. F. Lange, and D. S. Pearson, "New Method for Efficient Colloidal Particle Packing via Modulation of Repulsive Lubricating Hydration Forces," *Langmuir*, **6**, 1323–25 (1990).

[14] J. C. Chang, B. V. Velamakanni, F. F. Lange, and D. S. Pearson, "Centrifugal Consolidation of Al_2O_3 and Al_2O_3–ZrO_2 Composite Slurries vs

Interparticle Potentials: Particle Packing and Mass Segregation," *J. Am. Ceram. Soc.*, **74** [9] 2201–204 (1991).

[17]Y.W. Mai and A.G. Atkins, "Crack Stability in Fracture Toughness Testing," *J. Strain Anal.*, **15** [2] 63–74 (1980).

[18]M. Sakai and M. Inagaki, "Dimensionless Load-Displacement Relation and Its Application to Crack Propagation Problems," *J. Am. Ceram. Soc.*, **72** [3] 388–94 (1989).

[19]H. Tada, *The Stress Analysis of Cracks Handbook*, 2nd ed. Paris Productions Inc., St. Louis, MO, 1985.

[20]R.M. McMeeking and A.G. Evans, "Mechanics of Transformation Toughening in Brittle Materials," *J. Am. Ceram. Soc.*, **65** [5] 242–46 (1982).

[21]D.B. Marshall, A.G. Evans, and M. Drory, "Transformation Toughening in Ceramics", p. 289 in *Fracture Mechanics and Ceramics*, Vol. 6. Edited by R.C. Bradt, A.G. Evans, D.P.H. Hasselman, and F.F. Lange. Plenum Press, New York, 1983.

[22]A.G. Evans and R.M. Cannon, "Toughening of Brittle Solids by Martensitic Transformations," *Acta Metall.*, **34** [5] 651–800 (1986).

[23]A.G. Evans and D.B. Marshall, "The Mechanical Behavior of Ceramic Matrix Composites," *Acta Metall.*, **37** [10] 2607–83 (1989).

[24]W.J. Clegg, K. Kendall, N. McN. Alford, T.W. Button, and J.D. Birchall, "A Simple Way to Make Tough Ceramics," *Nature (London)*, **347**, 455–57 (1990).

[25]A.H. Heuer, M.J. Readey, and R. Steinbrech, "Resistance Curve Behavior of Supertough MgO-Partially-Stabilized ZrO_2," *Mater. Sci. Eng.*, **A105/106**, 83–89 (1988).

[26]M.J. Readey and A.H. Heuer, "Annealing of Test Specimens of High-Toughness Magnesia-Partially-Stabilized Zirconia," *J. Am. Ceram. Soc.*, **71** [1] C-2–C-6 (1988). □

MATERIALS

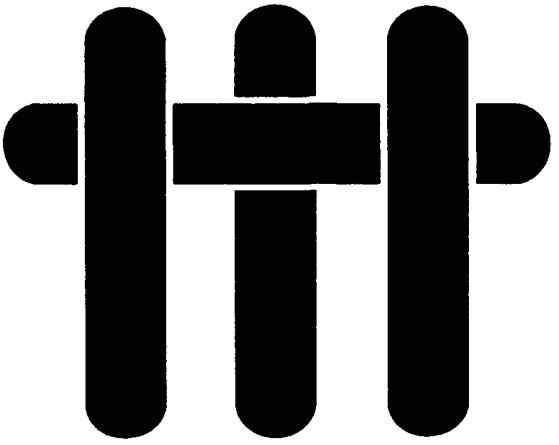

Technical Report Number 6

Correlation Between Random Dense Parking and Random Dense Packing for Determining Particle Coordination Number in Binary Systems

D. Bouvard and F. F. Lange

Office of Naval Research

Grant No. N00014-90-J-1441

Fred F. Lange and Dale S. Pearson

Principal Investigators

Materials Department
University of California
Santa Barbara, CA 93106

PHYSICAL REVIEW A VOLUME 45, NUMBER 2 15 JANUARY 1992

Correlation between random dense parking and random dense packing for determining particle coordination number in binary systems

D. Bouvard* and F. F. Lange

Materials Department, University of California, Santa Barbara, Santa Barbara, California 93106

(Received 29 July 1991)

An alternative method is proposed to estimate particle coordination number in a random packing of spheres. It is based on the correlation between random dense packing and random dense parking, where random dense parking is defined as the random placement of equal-size disks (or spheres) on a surface such that none overlap. Assuming that the limit for random dense parking (fraction of area covered by the projected area of particles) is independent of surface curvature, an analytical expression of the coordination number for spheres surrounding a central sphere of equal or different size is obtained. A similar analysis is achieved for a sphere touching a flat wall. Both expressions are tested through numerical simulations of bimodal, spherical particle systems.

PACS number(s): 82.70.Dd, 81.20.Ev

I. INTRODUCTION

The average coordination number of particles in a powder compact is an important parameter relevant to many problems that include powder packing density, the densification of metal and ceramic powders, connectivity problems (i.e., pressure transmission during deformation processing of particulate composites), and chemical engineering applications of powder coatings. Analytical models have been proposed [1,2] to predict coordination, supported by numerical simulations of random packing of sphere mixtures. Other research efforts [3–6] have been devoted to the problem of random dense parking, defined as the random placement of equal-size disks (or spheres) on a flat surface such that none overlap. Different experimental and numerical methods have been developed to estimate the random dense parking limit, that is "...the area fraction of a plane covered by circles when the circles are added sequentially in a random way, without overlap, until no further circles can be added" [6]. Using identical, colloidal, spherical particles that repel one another, but stick to a flat substrate, Onoda and Liniger [6] experimentally determined the random dense parking limit to be 0.55, whereas computer simulations [3–5] have given values between 0.5 and 0.55.

Although random dense parking is a concept used to understand the area fraction of a planar surface covered by the densest random arrangement of either disks or the projected area of spheres, it is conceivable that the same concept can be used for nonplanar surfaces. The physics relating the random dense parking limit for a flat surface to that of a curved surface is illustrated in Fig. 1. Let us assume that the limit for random dense parking has been achieved on a flat surface with the arrangement of spherical, identical particles shown in Fig. 1(a). In this arrangement, insufficient space is left to allow the shaded particle to join the surface (its projected area would overlap the projected areas of the adjacent, contacting spheres). Keeping all particles fixed to the surface, we now bend the surface until the increased interparticle spacing is sufficient to allow the shaded particle to join the surface as shown in Fig. 1(b). Although this bending has obviously increased the number of contacting particles per unit area, it can be seen from Figs. 1(c) and 1(d) that the projected area per particle (loci of tangents on the surface, drawn through the surface's center of curvature) decreases with the radius of curvature. With the assumption that the limit for random dense parking (fraction of area covered by the projected area of particles) is independent of surface curvature, the number of particles per unit area can easily be computed for any surface of known curvature.

With this same assumption applied to the surface of a sphere, one has the ability, detailed below, to determine the number of identical spheres of one size that can coordinate a central sphere of a second size for the condition of dense random parking. It is also conceivable that this concept might be valid for the case where spherical inclusions, isolated from one another at low volume fractions, are embedded in a random packing of other spherical particles to relate random dense parking to the coordination number achieved during random dense packing where simulation experiments can be used to test the proposed analytical expression. In addition, a related problem concerning the coordination number of an inclusion embedded in a powder which also touches the wall of container can be analytically modeled and tested through simulation. As detailed below, analytical expressions have been developed for the coordination number of a central

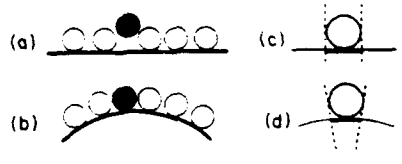

FIG. 1. Effect of surface curvature on the placement of spherical particles.

sphere surrounded by different identical spheres and a central sphere which both touches a flat wall and is also surrounded by other identical spheres. These expressions are then tested through numerical simulations of bimodal, spherical particle systems.

II. MODEL OF COORDINATION NUMBER

A. Spheres surrounding a central sphere

A bimodal mixture of spherical matrix particles of radius r_m and spherical inclusions of radius r_i is considered. When a matrix particle touches an inclusion its projected area is secured by the contact and therefore is no longer available for another contact (Fig. 2). This area fraction S_1 of the inclusion is easily calculated

$$S_1 = \frac{2\pi r_i^2(1-\cos\theta)}{4\pi r_i^2} = \frac{1-\cos\theta}{2}, \tag{1}$$

where θ is the angle defined in Fig. 2; that is

$$\sin\theta = \frac{r_m}{r_m + r_i} = \frac{R}{1+R}, \tag{2}$$

where R is the size ratio r_m/r_i. Thus

$$S_1 = \frac{1}{2}\left|1 - \frac{\sqrt{1+2R}}{1+R}\right|. \tag{3}$$

Assuming that the arrangement of particles on the surface of the inclusion is similar to the random dense parking of circles on a flat surface, one can estimate the coordination number for inclusions touching particles

$$Z_{im} = \frac{A_p}{S_1}, \tag{4}$$

where A_p is the random dense parking limit. Onoda and Liniger [6] experimentally found an upper limit $A_p = 0.55$, leading to

$$Z_{im} = \frac{1.1}{1 - \frac{\sqrt{1+2R}}{1+R}}. \tag{5}$$

When $R \ll 1$, that is, the inclusions are much larger than the particles, Eq. (5) simplifies to

$$Z_{im} = \frac{2.2}{R^2}. \tag{6}$$

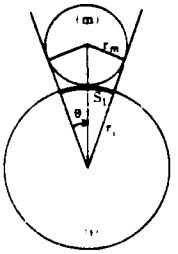

FIG. 2. Geometry of the contact between an inclusion and a matrix particle.

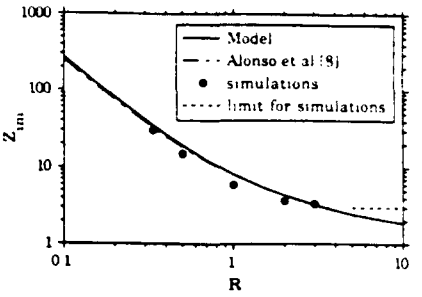

FIG. 3. Evolution of coordination as function of size ratio.

Figure 3 shows the evolution of Z_{im} as fraction of R, as predicted by Eq. (5). Z_{im} decreases as R increases and is 8.2 when $R = 1$.

B. Central sphere touching a flat wall

The packing of particles in a box is indeed perturbated by the walls of the box. The most studied effect has been the lower packing density observed close to the walls [7]. Numerical simulations show that the coordination number is also affected by the walls. This effect can be quantitatively estimated using an approach similar to that previously described.

The geometry of an inclusion touching a wall is shown in Fig. 4. The area fraction available for contacts with matrix particles is

$$S_2 = \frac{4\pi r_i^2 - 2\pi r_i^2(1-\cos\gamma)}{4\pi r_i^2} = \frac{1+\cos\gamma}{2}, \tag{7}$$

where γ is

$$\gamma = \frac{\pi}{2} - \theta - \varphi, \tag{8}$$

with

$$\sin\theta = \frac{R}{1+R} \tag{9}$$

and

$$\sin\varphi = \frac{1-R}{1+R}. \tag{10}$$

Combining the above expressions, the area fraction of the

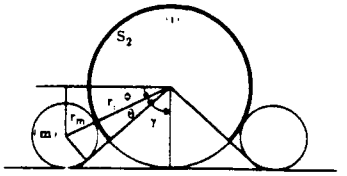

FIG. 4. Geometry of the contact between an inclusion touching a wall and a matrix particle.

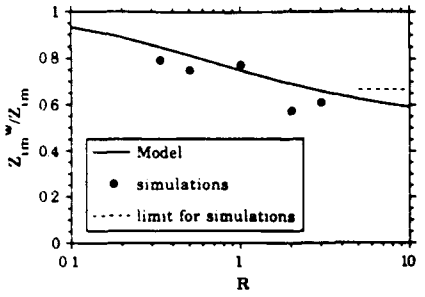

FIG. 5. Influence of wall on coordination.

inclusion available for the dense random parking of matrix particles is

$$S_2 = \frac{1}{2}\left[1 + \frac{2R\sqrt{R} + (1-R)\sqrt{1-2R}}{(1+R)^2}\right]. \tag{11}$$

Therefore the coordination number of inclusions touching a wall is

$$Z_{im}^{w} = S_2 Z_{im}. \tag{12}$$

The predicted ratio Z_{im}^{w}/Z_{im} is plotted as a function of R ($A_p = 0.55$) in Fig. 5. As shown, Z_{im}^{w}/Z_{im} decreases with increasing R. When $R \to 0$, $Z_{im}^{w}/Z_{im} \to 1$ and when $R = 1$, $Z_{im}^{w}/Z_{im} = 0.75$.

III. NUMERICAL SIMULATIONS

To test the coordination number models [Eqs. (5) and (12)] numerical simulations of bimodal powder mixtures, packing into a cubic box, were performed with different values of R between 0.33 and 3. Details of the procedure can be found in Ref. [2]. As a consequence of the packing algorithm, viz., each new particle added must make contact with three particles, the mean number of contacts per particle is exactly 6. This algorithm produces also a lower packing density (≈ 0.57 for monosized particles ($R = 1$) relative to that for random dense packing (≈ 0.64, $R = 1$).

For the current studies, simulations must be carried out for cases where the volume fraction of the inclusion spheres is sufficiently low such that the inclusions are isolated from one another (coordination number for inclusions touching one another equals zero). However, a sufficient number of inclusions is needed such that the estimation of coordination numbers is statistically significant, the total number of packed particles being limited to 10 000 due to computation time. With regard to first problem to be studied, viz., the coordination number of a central inclusion, these two opposing simulation requirements are fulfilled with a volume fraction of inclusions equal to 0.01 for $R < 1$ and 0.001 for $R > 1$. As the second requirement is particularly severe for the investigation of inclusions touching a wall, a higher volume fraction, 0.10, was selected. As discussed below, this value made the interpretation of the results somehow delicate. In the case $R = 1$, as indeed each particle can be considered as an inclusion or a matrix particle, there is no such difficulty.

The coordination number Z_{im} for inclusions touching particles in a central part of the box is compared in Fig. 5 to the prediction of Eq. (5). The agreement is reasonably good for any simulated size ratio, although the model systematically overestimates the numerical results.

For testing Eq. (12) other mixtures with a higher volume fraction of inclusions were used, as discussed above. The average coordination number Z_{im}^{w} of inclusions touching any wall of the box has been determined and compared to the value of Z_{im} stemmed from the simulations used to validate Eq. (5). As shown in Fig. 5, Eq. (12) overestimates the ratio Z_{im}^{w}/Z_{im}, except for $R = 1$.

IV. DISCUSSION

The coordination number model presented above agrees quite well with the numerical results within the range of R that can be conveniently simulated ($0.33 < R < 3$). However, the model systematically overestimates Z_{im} relative to the simulations which may, in part, be due to the deposition algorithm. For example, for $R = 1$ (monosized particles) it predicts a coordination number of 8.2, while this number is 6 in the simulated loose packing. Despite numerous studies, the coordination number in real, random dense packing has never been precisely measured due to the practical difficulty in distinguishing between close and near contacts [9]. Proposed values range from 6 to 9 [10]. Generally quoted literature values of 7.5 and 7.3 are based on estimates obtained by the linear extrapolation of radial distribution functions by Mason [11] and Artz [12], respectively, whereas computer simulations of dense random packing suggest a value closer to 6. Thus it might be concluded that the model (based on $A_p = 0.55$) overestimates the coordination number of an inclusion within a dense random packed system by about 10%. For $R > 3$, the model is invalid since the minimal number of contacts required for mechanical stability in particle packing is 3, as shown in Fig. 3.

As an additional evaluation of Eq. (5) the results obtained by Aloson, Satoh, and Miyanami [8] have been plotted in Fig. 2. Their empirical model is based on a constant distance between adjacent particles that contact the central sphere, leading to

$$Z_{im} = \frac{2\pi}{\sqrt{3}\lambda^2}\left[1 + \frac{1}{R}\right]^2 \tag{13}$$

for $R \leq 1$, where λ is the center-to-center distance of adjacent particles in unit of particle diameter. λ is used as an empirical fitting parameter, which is adjusted to fit their computer simulations of random placements of particles on a central sphere. With $\lambda = 1.33$, the model fits perfectly to their simulations. As shown in Fig. 3 these results are very close to the predictions of Eq. (5) in the

range of size ratio $R \leq 1$. Indeed, for $R \ll 1$, Eq. (12) gives, with $\lambda \approx 1.33$,

$$Z_{im} = \frac{2.05}{R^2} , \tag{14}$$

which agrees very well with Eq. (6).

Although the model is in good agreement with the simulations for isolated inclusions with a three-dimensional system, the agreement is less perfect for inclusions touching a wall. As pointed out above, in the simulations used for the determination of Z_{im}^{w}, the volume fraction of inclusions was chosen so that a significant number of inclusions touch the wall. Because of the higher volume fraction of inclusions in these simulations, although the inclusions do not touch one another, many are closely spaced. As a consequence some matrix particles are excluded from packing between the closely spaced, but nontouching inclusions. This effect may explain the discrepancy between the model and the simulations. In addition, for $R \gg 1$ most inclusions touch three particles, whereas the inclusions touching a wall need only two additional contacts. Hence, when $R \gg 1$, $Z_{im}^{w}/Z_{im} \approx \frac{1}{3}$, which sets the expected lower limit shown by the dashed line in Fig. 5.

V. CONCLUSIONS

The model of coordination obtained by comparing the placement of spherical particles around a central sphere to the random dense parking of disks on a flat surface satisfactorily fits the results of numerical simulations, even when the central sphere is smaller than the contacting particles. The coordination number of a sphere touching a wall has been also studied, but the comparison is not so good, likely because of the poor suitability of numerical packing statistics to this particular problem. It is thought that the correlation displayed in this paper can be very useful to tackle other problems of coordination in various systems.

ACKNOWLEDGMENTS

D. B. thanks Direction des Etudes, Recherches et Techniques of Délégation Générale pour l'Armement for supporting his stay at UCSB jointly with Centre National de la Recherche Scientifique. Both workers acknowledge the support from U. S. Office of Naval Research Grant No. ONR N00014-90-J-1441. The Institut de Mécanique de Grenoble is "Unite Mixte de Recherches CNRS-UJF-INPG."

*Permanent address: Institut de Mecanique de Grenoble, BP 53X, 38041 Grenoble, France.

[1] L. Oger, J. P. Troadec, D. Bideau, J. A. Dodds, and M. J. Powell, Powder Tech. **46**, 121 (1986).

[2] D. Bouvard and F. F. Lange, Acta Metallog. Mater. (to be published).

[3] L. Finegold and J. Dunnel, Nature **278**, 443 (1979).

[4] M. Tanemura, Ann. Inst. Stat. Math. **31**, 351 (1979).

[5] J. Feder, J. Theor. Biol. **87**, 237 (1980).

[6] G. Y. Onoda and E. G. Liniger, Phys. Rev. A **33**, 715 (1986).

[7] R. Ben Aim and P. Le Goff, Powder Tech. **1**, 281 (1967).

[8] M. Alonso, M. Satoh, and K. Miyanami, Powder Tech. **62**, 35 (1990).

[9] J. D. Bernal and J. Mason, Nature **188**, 910 (1960).

[10] R. M. German (unpublished).

[11] J. Mason, J. Colloid Interface Sci. **35**, 75 (1971).

[12] E. Artz, Acta Metallog. **30**, 1883 (1982).

MATERIALS

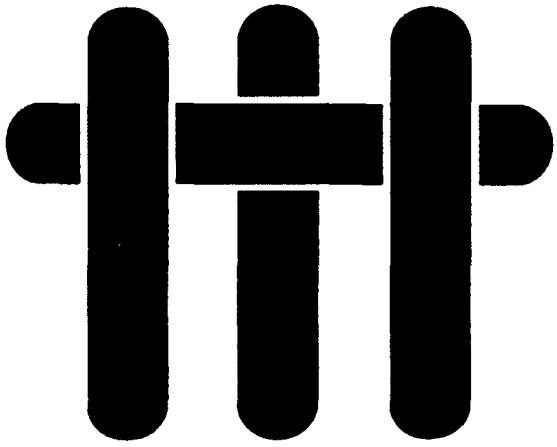

Technical Report Number 7

The Viscosity and Yield Stress of Al2O3 Slurries Containing Large Concentrations of Electrolyte

Jeanne C. Chang, F. F. Lange and D. S. Pearson

Office of Naval Research

Grant No. N00014-90-J-1441

Fred F. Lange and Dale S. Pearson

Principal Investigators

Materials Department
University of California
Santa Barbara, CA 93106

Abstract

Viscosity and yield stress measurements of Al_2O_3 slurries containing high concentrations of electrolyte are reported. Contrary to what is expected from DLVO theory, the particles in coagulated slurries produced in this way are held together by weaker forces than particles in slurries brought to the isoelectric point by changing the pH. In both cases an attractive, connective particle network is present. However, the network at the isoelectric point is stronger, as indicated by its much higher yield stress and by its higher viscosity at stresses above the yield point. An additional short-range repuslsive force that appears at low pH and high electrolyte concentrations is believed to be responsible. This force prevents the particles from reaching the primary minimum associated with particle contact. The effect of solids loading, electrolyte concentration and type, and particle size have been investigated.

I. Introduction

Colloidal processing methods have been suggested[1,2,3] as a method of preparing advanced ceramic materials with improved mechanical and electrical properties. In this process, a ceramic powder is first dispersed in a liquid where the interparticle potentials have been adjusted to provide repulsive interactions. Weakly bound agglomerates are broken apart with intense mixing techniques such as ultrasonication, and strongly bound agglomerates, large particles, and other foreign material are removed by either sedimentation or filtration. Once these heterogeneities have been separated, the slurry conditions are adjusted so that the interparticle potentials are weakly attractive. The material now forms a network in which particles of different mass do not differentially settle. The attractive interactions have another advantage. Once the slurry is consolidated by centrifugation or filtration into a dense body, the attractive interactions

provide the mechanical strength needed to hold the body shape until sintering occurs.

An aqueous slurry with long-range, electrostatic repulsive potentials can be destabilized by one of two methods: 1) the pH can be adjusted to the particle's iso-electric point or 2) an electrolyte can be added until the electrostatic potential has been screened by counterions. In this paper we refer to the former case as flocculation and the later as coagulation. Until recently, it was not realized that important differences exist in these two ways of processing alumina.[2] Coagulated slurries are unique in that they have yield stresses, high viscosities, and shear thinning characteristics similar to flocced slurries, but unlike flocced slurries, they can be packed at lower pressures to a density similar to that achieved with dispersed slurries.[4] Thus, coagulated slurries offer a great potential for improving the colloidal processing of ceramics in that mass segregation effects are eliminated and consolidated body strength is achieved without sacrificing efficiency in particle packing. It is clear that a better understanding of this state is required to fully exploit its use in the processing of other types of ceramics.

Similarities in the rheological behavior of coagulated alumina slurries and clay slurries indicates that a short-range, hydration potential may be responsible for their unique properties.[5] The existence of such a potential was demonstrated by Israelachvili and Adams[6] and Pashley and Israelachvili[7] for cleaved mica surfaces. However, with the exception of our initial report[2], little is known about the differences in rheological behavior of coagulated and flocced slurries. Thus, the purpose of this work was to study the rheological and consolidation behavior of coagulated alumina slurries, and to see if the results are consistent with the existence of an additional short-range, repulsive interparticle potential due to hydrated surfaces.

II. Experimental Procedure

(1) Materials and Preparation of Slurries

Aqueous slurries were prepared by mixing α-Al_2O_3 particles with deionized water which had a conductance of 14 megaohm-cm. Two different α-Al_2O_3 powders[a] , designated AKP-50 and AKP-15, were investigated. The AKP-50 powder, used for most experiments, had an average particle diameter of 0.20 microns[b] , a specific surface area of 9.9 m^2/g[c] and a density of 3.94 g/cm^3. The AKP-15 powder, used for several experiments to investigate size effects, had an average particle size of 1.0 micron[b]. As reported elsewhere,[2] the zeta potential for these powders is positive at low pH and decreases to zero at a pH between 8 and 9. The slurries were initially dispersed at pH 4 by ultrasonicating 30 ml in 50 ml container at 95 W for 10 minutes[d] prior to addition of salt or further pH adjustments. Alumina slurries prepared at lower pH tend to drift upward towards pH = 4 as a function of time.

All pH adjustments were made by adding either HNO_3 or NH_4OH. Settling experiments were performed using 0.10 volume fraction AKP-50 Al_2O_3 slurries at pH 4 containing different concentrations of NH_4Cl, to determine the minimum salt concentration required to produce an attractive particle network; the value of the critical coagulation concentration (ccc) was determined from this to be 0.12 M. When salt was added, it was first dissolved in water, and the initial volume fraction of slurry was chosen so that after the salt was added the final desired volume fraction of 0.10, 0.20, and 0.30 was attained. Although most

---

[a] Sumitomo Chemical Co., New York
[b] Micromeretics Sedigraph 5000ET, Norcross GA
[c] Micromeretics Accelerated Surface Area and Porosimetry System 2000, Norcross, GA.
[d] Ultrasonic Liquid Processor W-380, Heat Systems-Ultrasonics, Inc., Farmingdale, NY

studies were carried out with NH_4Cl, the comparative effects of KI and NH_4NO_3 were also studied for 0.20 volume fraction slurry of AKP-50 powder.

(2) Viscosity vs. Shear Rate Measurements

The steady state viscosity was measured as a function of shear rate using rheometers[e,f] operating in constant rate mode. High viscosity slurries were measured[e] in either a coni-cylinder and cup (2° cone, 1 mm gap, 74.4 mm length, 25.2 mm cylinder diameter), a couette and cup (1 mm gap, 74.4 mm length), or a parallel plate geometry (50 mm diameter, 2 mm gap). All measurements of low viscosity slurries were performed[f] in a cup and bob (1 mm gap, 91 mm length, 27.5 mm diameter cup or 40 mm length and 18.9 mm diameter cup) geometry. For all viscosity vs. shear rate experiments the following procedure was used. After a slurry was prepared, its pH was measured and adjusted if necessary before loading it into the rheometer. It was then sheared for two minutes at 10/s followed by five minutes at rest. The viscosity was measured by first stepping up in shear rate and then stepping down, followed by second step up and a final step down. Measurements were taken at five shear rates per decade equally spaced on a logarithmic scale. At each shear rate, the sample was sheared for 30 seconds in one direction before the average stress was determined during the next 30 seconds. The shearing direction was then reversed and the procedure repeated. Thus, each point represents the average of measurements in two shear directions, and only measurements made while stepping down in shear rate were used. By monitoring the stress level continuously with a chart recorder, it was determined that steady state was essentially reached in all of our measurements. Evaporation of water was minimized while using the coni-

[e] Rheometrics RMS-800 supplied with a 2000g-cm transducer, Piscataway, NJ
[f] Brookfield Viscometer Model DV-II (full scale torque, 673.7 dyne/sq.cm.), Stoughtan, MA

cylinder and couette geometry by attaching an evaporative dish fixture which encased the upper part of the tool and provided a reservoir of water as shown in Figure 1. The additional torque from this device was negligible compared to the torque required to shear the sample.

(3) Yield Stress Determinations

Yield stress determinations for most slurries were made with a constant stress rheometer[8] using a coni-cylinder and cup geometry(2.4° cone, 1 mm gap, 60 mm length, 22 mm cylinder diameter). For these measurement the slurries were stirred for a minimum of 24 hours and their pH was measured prior to loading into the rheometer. Once loaded, the sample was left undisturbed for a minimum of one hour before increasing the shear stress at a rate of 0.20 Pa/s. The strain was recorded as a function of time and the strain rate was calculated at the conclusion of the experiment.

Others[8,9] have measured the yield stress by a variety of methods. Quite often the Bingham plastic model, which assumes a linear relationship between shear stress and shear rate, is used to extrapolate a yield stress value.[10] However, in cases in which the shear stress - shear rate is non-linear, such extrapolations can lead to an overestimate of the yield stress.[9] A variety of models which attempt to determine the yield stress from non-linear shear stress - shear rate curves have been developed and reviewed.[9,11,12] Of these models, the Casson model[13] described by equation (1) has been shown to provide a reasonable estimate of the yield stress as compared to other methods of measurement,[9] which was true in the case of our experiments as well.

---

8 Rheometrics RSR, Piscataway NJ

$$\tau^{1/2} = m\dot{\gamma}^{1/2} + \tau_y^{1/2} \qquad (1)$$

Reproducibility in our use of the method was determined by repeating the measurement on the same slurry after allowing it to rest for one hour in the rheometer, and by repeating the experiment on an identical, new slurry.

Flocculated slurries have a sufficiently high yield stress and viscosity so that they can not be conveniently loaded into a couette cell. Furthermore, the higher stresses generated suggested that wall slip might affect the accuracy of our results. For these materials, a vane tool similar to that described by Boger[9] was made to measure the yield stress of slurries at the isoelectric point (pH9). The vane, shown in Figure 2, was designed with a diameter of 2.5 cm and a length of 3.6 cm, and the cup was 5.4 cm in diameter and 7.4 cm deep. The same evaporative dish described earlier was also used with this geometry. The flocculated slurries were prepared by pouring a dispersed 0.20 volume fraction pH 4 slurry into the cup and then increasing the pH to 9, before lowering the vane into the slurry. The flocculated slurry was then sheared at a given rate while continuously measuring the torque.[e] As the slurry is sheared, the torque rises to a maximum value and then decreases to a plateau value. The maximum value has been shown by Dzuy and Boger to be independent of shear rate and to agree with the yield stress measured by other techniques.[9] The yield stress of a 0.20 volume fraction slurry at pH 4 with 2.0 M NH_4Cl was determined using both the coni-cylinder and cup and the vane and cup techniques in order to compare the two methods.

III. Experimental Results

(1) Viscosity vs. Shear Rate

In general, the viscosity obtained for shear thinning slurries was either the same or slightly lower while the shear rate was being stepped-up relative to when it was stepped-down. In some cases, the slope of the viscosity curve had rather abrupt changes in slope at different shear rates. The largest slope changes were observed for the flocced (pH 9) slurry containing 0.20 volume fraction AKP-50 powder (Figure 3b). At around 0.1/s an instability occurred where the logarithmic derivative of the apparent viscosity decreased with a slope less then -1 which indicates that the shear stress is actually decreasing with increasing shear rate. Between 0.1/s and 10/s the rate of change of the viscosity was the same as in the shear rate regions at higher and lower shear rates. Above 10/s the viscosity actually increased slightly before it started to fall again. Although we do not have an explanation for this behavior (the rapid decrease in viscosity was probably due to wall slip), it was reproducible. For the other samples where the viscosity was well behaved, the coagulated samples have a power law dependence of viscosity on shear rate that is remarkably constant. (See discussion below).

Figures 3a, 3b, and 3c illustrate the viscosity vs. shear rate results for slurries containing different volume fractions (0.10, 0.20, and 0.30) of AKP-50 Al_2O_3 at pH 4 (± 0.2) and with different concentrations of NH_4Cl. Figures 3a and 3b also report the rheological behavior for the flocced slurries (flocced slurries containing 0.30 volume fraction never reached steady state values during strain rate ramping, and are therefore not shown in Figure 3c). All curves were averaged from 2 or more different measurements at the reported slurry conditions. The following common features seem to be independent of the Al_2O_3 volume fraction:

a) The viscosities of dispersed slurries (pH 4) without added salt were low and relatively independent of shear rate, indicating a nearly Newtonian behavior.

b) All slurries at pH 4 with added salt had viscosities that decreased strongly with increasing shear rate. At the highest salt concentrations studied the power law slope was between 0.8 and 0.9.

c) The viscosity of pH 4 slurries increased with the salt concentration up to a maximum concentration where further additions had no effect on slurry rheology. The maximum salt concentration determined in this way is given in Table 1.

d) Flocced slurries exhibited stronger shear thinning behavior and had a much higher viscosity relative to coagulated slurries when compared at the same volume fraction.

Figure 4 summarizes the effect of increasing volume fraction (AKP-50 Al_2O_3, pH 4) for dispersed (no salt) slurries and coagulated slurries containing the salt concentration beyond which further addition of salt had no influence on the rheological behavior. As expected, increasing the volume fraction of the powder increases viscosity. Note also that the shear rate dependence of the viscosity and the salt concentration required to reach the maximum increases slightly with volume fraction (Table 1).

Similar rheological behavior (summarized by points a) through d) above) were obtained for slurries prepared at pH 2 and 6 (slurries were only prepared containing 0.20 volume fraction Al_2O_3). Figure 5 summarizes these results with viscosity vs. shear rate data for slurries containing no added salt and for those containing the concentration of salt at which further additions did not change the rheological behavior. Note that the this salt content decreases slightly with increasing pH (Table 1). For comparison, it can be seen that the viscosity of the flocced slurry (pH 9) is always greater than the coagulated slurries. Figure 6 shows that the effect of KI and NH_4NO_3 is similar to NH_4Cl. However, the maximum salt content required to reach the point where further additions have

no effect on rheological behavior appears to increase slightly with the size of the counter-ion, Cl^-(0.33 nm) < I^- (0.33 nm) < NO_3^- (0.34 nm) (See Table I).

Figure 7 illustrates the very important conclusion that salt additions have no effect on the rheological behavior of flocced (pH 9) slurries. If short range hydration forces are responsible for the observed effects, they apparently are not present or important at the isoelectric point.

The effect of particle size on the viscosity of pH 4, 0.20 volume fraction slurries (with and without salt) made with AKP-50 and AKP-15 Al_2O_3 powders is shown in Figure 8. As can be seen, the viscosity of 0.20 volume fraction slurries made with AKP-15, the larger powder, is consistently lower than that of 0.20 volume fraction slurries made with AKP-50. However, the slope of log η vs. log $\dot{\gamma}$ for both systems is similar. Furthermore, as in the case of the AKP-50 slurries, there is a salt concentration beyond which the viscosity of the AKP-15 slurries does not increase any further.

(2) Yield Stress Measurements

Figure 9a shows a typical stress-shear rate curve for yield stress determinations, and in Figure 2.9b is the corresponding Casson plot. In all cases, there was essentially no measurable strain until a certain stress level was exceeded. Beyond this point the shear rate increased nonlinearly with the applied stress until the maximum shear rate of the instrument was reached (about 25/s with this sample cell). As can be seen the Casson equation was not completely satisfactory in describing the slurry behavior. It is possible, however, that a better fit may have been found had higher shear rates been explored. Nonetheless, the calculated value from the Casson plot appeared to be consistent with a value which might be directly extrapolated from the shear stress-shear rate data.

Figure 10 shows yield stresses obtained as a function of NH_4Cl concentration for slurries at pH 4 containing 0.10, 0.20, 0.30 and 0.40 volume fraction of AKP-50. It also shows a single point showing the yield stress of the flocced (pH 9) slurry. Because of limitations on the maximum stress that the constant stress rheometer can apply and evidence that wall slip occurs at high stresses, the yield stress measurements for the 0.30 and 0.40 volume fraction slurries were limited to low concentrations of salt. The yield stress of the flocced slurry (0.20 volume fraction powder, pH 9) was measured with the vane tool on a constant displacement rheometer. In order to compare the two methods of measurement, the yield stress of a 0.20 volume fraction slurry containing 2.0 M NH_4Cl at pH 4 was measured with both techniques. The vane and cup method produced a higher value (14 Pa) relative to the coni-cylinder and cup method (9 Pa), but the difference is not significant compared to other changes we observed (see Figure 10).

The yield stress behaves in a manner similar to the viscosity. With increasing salt concentration it reaches a plateau value, beyond which any further salt does not effect the yield stress. As indicated in Table 2, the maximum electrolyte concentration that resulted in a yield stress plateau was somewhat different (± 0.3M NH_4Cl) than that found for viscosity measurements. The yield stress of the flocced slurry containing 0.20 volume fraction of powder was more than an order of magnitude greater than the coagulated slurries.

IV. Discussion

The shear thinning behavior of the coagulated and flocced slurries indicates that the particles form a connected network that can be broken apart by shearing. Michaels and Bolger[14], Firth and Hunter[10,15], and Hoffman[16] discussed this concept in the context of flocculated slurries. They suggested that a

connected particle network exhibits a large viscosity beyond the yield stress because both the network and its entrapped liquid must be moved to induce flow. Viscosity decreases when the network is sheared because it is broken into smaller and smaller flow units. The shear rate required to achieve a given viscosity is indicative of the work required to break apart the network and produce a certain average flow unit size. It can be expected that the strength of this network, viz., how difficult it is to break it apart into smaller flow units, will depend on the magnitude of the attractive force between particles, the volume fraction of particles, and the network connectivity or structure.

Both viscosity vs. shear rate data and yield stress measurements show that when salt is added to slurries at pH 4, the strength of networks formed increases to a maximum value that is significantly less the strength of networks at pH 9. In addition, although the strength of these attractive networks can be very different, the shear rate dependence of viscosity is nearly identical and independent of the particle volume fraction, particle size, and how the networks were formed. Their similar shear rate dependency suggests that all of the attractive networks have a similar structure with different strengths. Although the details of the network structure have not been determined yet, the network strength should be related to the interparticle potentials.

Relating the properties of aqueous Al_2O_3 slurries to interparticle potentials should begin with a discussion of the theory due to Derjaguin and Landau[17] and Verwey and Overbeek (DLVO).[18] The theory assumes that the total potential is the sum of a repulsive part, V_R, electrostatic in origin, and an attractive part due to van der Waals forces, V_A:

$$V_T = V_A + V_R \tag{2}$$

Alumina particles in water are strongly attracted to each other as indicated by their large Hamaker constant[19] of 16.2 kT. However, when V_R is sufficiently

large, a potential barrier greater than kT keeps the particles from forming an attractive network. This condition occurs when the pH has been adjusted below (or above) the isoelectric point and when the range of forces as indicated by the Debye screening length is large. In this case the particles are repelled from each other and they flow as individual units. The viscosity is essentially Newtonian under these conditions.

According to DLVO theory V_R can made to approach zero either by adding sufficient electrolyte (salt) to screen the charged sites or by changing the pH to the particle's isoelectric point. In either case, the particles are expected to fall into a primary minimum and form a cohesive, touching particle network. We previously determined[2] that the isoelectric point of the α-Al_2O_3 we are using occurs at a pH between 8.5-9, and the zeta potential is at a maximum of approximately 40 mV at a pH between 2 and 4. Both results are in agreement with values reported by others.[19] In this pH range the particles are expected to be repulsive, act as individual flow units and produce a low viscosity, nearly Newtonian slurry as reported above.[20] A pH of 9 produces a strongly attractive particle network with a high viscosity that shear thins as reported above. Lowering the pH to 6 is enough to produce a low viscosity dispersion with near Newtonian behavior. These findings are in qualitative agreement with DLVO theory.

Because the repulsive potential barrier can be eliminated by either high electrolyte concentrations or going to the isoelectric point, the effect that we have observed by adding salt is not consistent with the DLVO theory. We believe that a third, short-range repulsive potential as suggested in our earlier paper[2] is responsible for the difference. This type of potential is produced when hydrated counterions are attracted to the positive surface sites on Al_2O_3 when the pH < 8, to form a layer of structured water bound to the surface by the counterions. The

short-range repulsive potential is thus called a hydration potential, which is only effective, relative to the other potentials, when the interparticle separation distance is on the order of 5 nm or less. When the amount of salt added is insufficient to remove the electrostatic potential barrier, the short-range repulsive potential will have little or no effect on slurry rheology. Likewise, when the number of charged surface sites is small, there will be insufficient counterions to form the hydration layer, and the magnitude of the short-range repulsive potential will be close to zero. Adding salt to a slurry close to its isoelectric point has little or no effect on the rheology of flocced slurries as shown in Figure 7.

It is believed that the thickness of the hydration and double layer is independent of particle size. Since particles will resist interpenetrating their exterior layers, an effective volume fraction may be calculated by considering the particle radius to be $a+\Delta$, where Δ represents the thickness of the layers and is independent of particle size. This implies that at any given true volume fraction, a system of small particles will have a larger effective volume fraction than a system of large particles. It has been shown that the viscosity increases with increasing volume fraction.[21] Thus, a system of smaller particles is likely to have a higher viscosity than the system of larger particles, as was found in the case of slurries made from AKP-50 (0.20 μm diameter) as compared to slurries made from AKP-15 (1.0 μm).

The effect of a short-range repulsive hydration potential on an Al_2O_3 slurry will only occur when the particles are charged (e.g., pH < 8) and when the amount of salt added is sufficient to produce the hydration layer and to decrease the electrostatic potential barrier to allow particles to come into closer contact. The range of salt concentrations where the short-range hydration potential can effect the network strength is between the critical coagulation concentration and

the salt concentration we found to bring the viscosity and yield stress to their maximum values. Within this range, the depth of the force of attraction increases with increasing salt content, but never become as strong as expected for the van der Waals potential alone. With this hypotheses, the increasing strength of the Al_2O_3 particle networks formed at salt concentration above the ccc and the observation that theses networks are weaker that those formed by going to the isoelectric point can be explained. In the future we hope to learn more about the nature of these short range forces by direct measurement in the surface force apparatus or an atomic force microscope, and then use this information to further our understanding of the rheological behavior.

V. Conclusion

Viscosity and yield stress measurements of positively charged, dispersed Al_2O_3 slurries (pH 2 to 6) that contain up to 2.2 M electrolyte are reported. Our results indicate that these systems do not behave the same as slurries at the isoelectric point (pH 9). Although our finding are not in agreement with DLVO theory, it is suggested that a resolution is possible if a short range repulsive force is present. According to this scenario, the particles are attracted to each other by van der Waals forces, but hydrated counterions, which are believed to be responsible for the short range forces, prevent the particles from coming into direct contact. Such hydrated layers do not form at the isoelectric point and hence the yield stress and viscosity of networks formed at the isoelectric are up to an order of magnitude higher. The ability to form networks which can easily be arranged with moderate stresses is expected to play an important role in ceramic processing.

Acknowledgements

The authors would like to thank Dr. Bhaskar Velamakanni for his assistance, and the Office of Naval Research for the their support of this work under contract #N00014-90-J-1441 .

References

[1] Lange, F. F., "Powder Processing Science and Technology for Increased Reliability, " *J. Am. Ceram. Soc.*, **72(1)**: 3-15, 1989.

[2] Velamakanni, B. V., Chang, J. C., Lange, F. F., and Pearson, D. S., "New Method for Efficient Colloidal Particle Packing via Modulation of Repulsive Lubricating Hydration Forces," *Langmuir*, **6**: 1323-1325, 1990.

[3] Cameron, C.P. and Raj, R. "Better Sintering through Green-State Deformation Processing", *J. Am. Ceram. Soc.*, **73(7)**: 2032-2037, 1990.

[4] Chang, J. C., Lange, F. F., and Pearson, D. S., "Compaction of Al_2O_3 Slurries by Centrifugation: The Effect of Interparticle Potentials," to be submitted.

[5] Israelachvili, J. N., "Measurements of Hydration Forces between Macroscopic Surfaces, " *Chemica Scripta*, **25**: 7-14, 1985.

[6] Israelachvili, J. N., and Adams, G. E., "Measurement of Forces between Two Mica Surfaces in Aqueous Electrolyte Solutions in the Range 0-100 nm," *J. Chem. Soc. Faraday Trans. I*, **74**: 975-1001, 1978.

[7] Pashley, R. M., and Israelachvili, J. N., "Molecular Layering of Water in Thin Films between Mica Surfaces and Its Relation to Hydration Forces," *J. Colloid and Interface Science*, **101(2)**: 511-523, 1984.

[8] Avramidis, Kostas S., and Turian, Raffi M., "Yield Stress of Laterite Suspensions," *J. Colloid and Interface Science*, **143(1)**: 54-68, 1991.

[9] Dzuy, N. Q., and Boger, D. V., "Yield Stress Measurements for Concentrated Suspensions," *J. of Rheology*, **27(4)**: 321-349, 1983.

[10] Firth, B. A. and Hunter, R. J., "Flow Properties of Coagulated Colloidal Suspensions, I. Energy Dissipation in the Flow Units," *J. Colloid and Interface Science*, **57(2)**: 248-256, 1976.

[11] Doraiswamy, D., Mujumdar, A. N., Tsao, I., Beris, A. N., Danforth, S. C., and Metzner, A. B., "The Cox-Merz Rule Extended: A Rheological Model

for Concentrated Suspensions and Other Materials with a Yield Stress," *J. Rheology*, **35(4)**: 647-685, 1991.

[12] Keentok, M., "The Measurement of the Yield Stress of Liquids," *Rheologica Acta*, **21**: 325-332, 1982.

[13] Casson, N. "A Flow Equation for Pigment-Oil Suspensions of the Printing Ink," in *Rheology of Disperse Systems*, C. C. Mills, ed., Pergamon Press, NY, 1959, p84.

[14] Michaels, A. S. and Bolger, J. C., "The Plastic Flow Behavior of Flocculated Kaolin Suspensions," *Ind. Eng. Chem. Fundam.*, **1(3)**:153-162, 1962.

[15] Firth, B. A. and Hunter, R. J., "Flow Properties of Coagulated Colloidal Suspensions, III. The Elastic Floc Model," *J. Colloid and Interface Science*, **57(2)**: 266,275, 1976.

[16] Hoffman, R. L., "Rheology of Concentrated Latexes and Dispersions," in *Science and Technology of Polymer Colloids, v.2*, G. W. Poehlein R. H. Ottewill, and J. W. Goodwin eds., series E-No 68, Nishoff, Boston, 1983.

[17] Derjaguin, B. and Landau, L., "Theory of the Stability of Strongly Charged Lyophobic Sols and of the Adhesion of Strongly Charged Particles in Solutions of Electrolytes," *Acta Physiochim URSS*, **14**: 633-662, 1941.

[18] Verwey, E. J. W. and Overbeek, J. Th. G., *Theory of the Stability of Lyophobic Colloids*, Elsevier, Amsterdam, 1948.

[19] Horn, R. G., Clarke, D. R., and Clarkson, M. T., "Direct Measurement of Surface Forces Between Saphire Crystals in Aqueous Solutions," *J. of Materials Research*, **3**: 413-416, 1988.

[20] Krieger, I. M., "Polymer Colloids as Model Systems for Studying Rheology of Dispersions, " in *Future Directions in Polymer Colloids*, M. S. El-Aasser and R. M. Fitch, eds., Martinus Nijhoff Publishers, Dordrecht, 1987, 119-130.

[21] Woods, M. E., and Krieger, I. M., "Rheological Studies on Dispersions of Uniform Colloidal Spheres, I. Aqueous Dispersions in Steady Shear Flow," *J. Colloid and Interface Science*, **34(1)**: 91-99, 1970.

Table 1. Salt concentration at which the viscosity reaches a maximum.

	Volume Fraction		
pH & Salt	0.10	0.20	0.30
pH2, NH_4Cl	---	1.875M	---
pH4, NH_4Cl	1.67M	1.70M	1.79M
pH6, NH_4Cl	---	1.25M	---
pH4, KI	---	1.875M	---
pH4, NH_4NO_3	---	2.19M	---

Table II. Salt concentration at which the yield stress reaches a maximum.

	Volume Fraction	
	0.10	0.20
Viscosity	1.67M	1.70M
Yield Stress	1.50M	2.0M

Figure 1. Coni-cylinder geometry showing seal designed to eliminate evaporation.

Figure 2. Vane tool used in yield stress measurements when the stress was high.

Figure 3a. Viscosity as a function of shear rate for 0.10 volume fraction Al_2O_3 slurries at pH 4 with and without NH_4Cl and at pH 9 without NH_4Cl.

Figure 3b. Viscosity as a function of shear rate for 0.20 volume fraction Al_2O_3 slurries at pH 4 with and without NH_4Cl and at pH 9.

Figure 3c. Viscosity as a function of shear rate for 0.30 volume fraction Al_2O_3 slurries at pH 4 with and without NH_4Cl.

Figure 4. Viscosity as a function of shear rate for 0.10, 0.20, and 0.30 volume fraction Al_2O_3 slurries at pH 4 without any salt additions, and with NH_4Cl concentrations which yield a maximum in viscosity.

Figure 5. Viscosity as a function of shear rate for 0.20 volume fraction Al_2O_3 slurries at pH 2, 4, and 6 without any salt additions, and with NH_4Cl concentrations which yield a maximum in viscosity, and at pH 9.

Figure 6. Viscosity as a function of shear rate for 0.20 volume fraction Al_2O_3 slurries at pH 4 without any salt additions, and with NH_4Cl, KI, and NH_4NO_3 concentrations which yield a maximum in viscosity.

Figure 7. Viscosity as a function of shear rate for 0.20 volume fraction Al_2O_3 slurries at pH 9 with and without NH_4Cl.

Figure 8. Viscosity as a function of shear rate for 0.20 volume fraction Al_2O_3 made with AKP-50 (.20μm diameter) and with AKP-15 (1.0μm diameter) powder. Slurries are at pH 4 and contain 0, 0.16 or 1.5 M NH_4Cl.

Figure 9a. Stress vs. strain rate plot obtained during a yield stress measurement of a 0.20 volume fraction Al_2O_3 slurry at pH 4 with 1.0 M NH_4Cl.

Figure 9b. Casson plot of the 0.20 volume fraction Al_2O_3 slurry at pH 4 with 1.0 M NH_4Cl shown in Figure 9a. The linear least squares fit predicts τ_y to be 4.46.

Figure 10. Yield stress of 0.10, 0.20, 0.30, and 0.40 volume fraction Al_2O_3 slurries at pH 4 with varying concentrations of NH_4Cl, and a 0.20 volume fraction Al_2O_3 slurry at pH 9. Measurements made using a vane tool are noted in inset. The solid lines are meant to guide the eye.

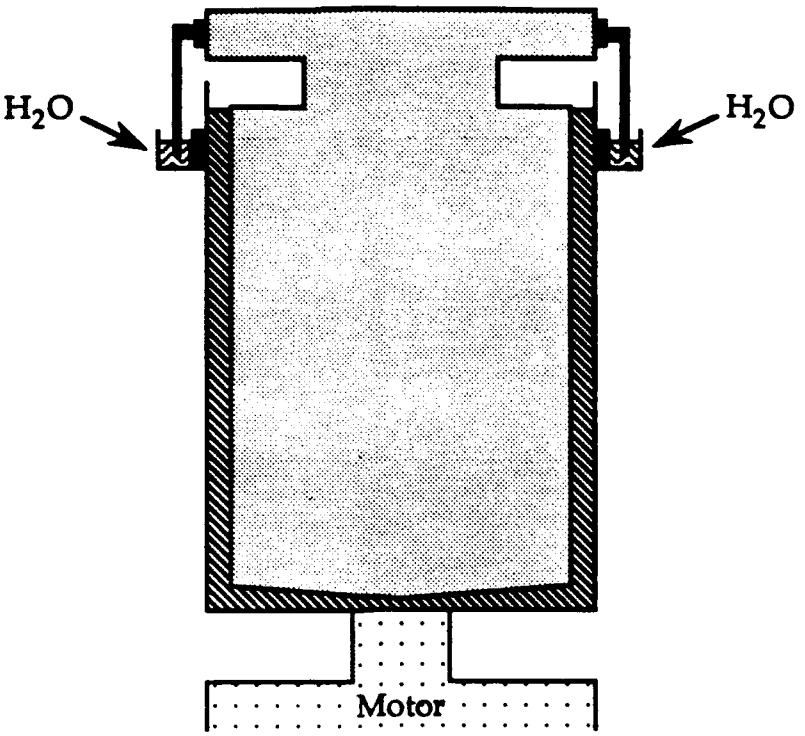

Figure 1

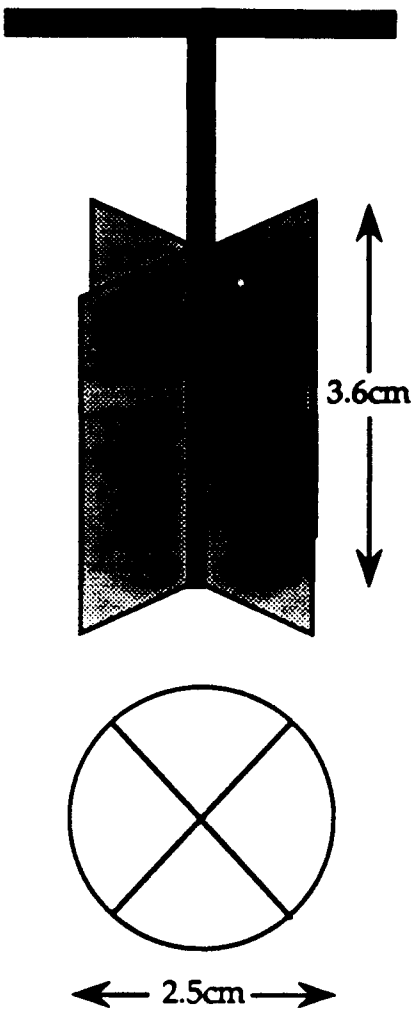

Figure 2

Figure 3b

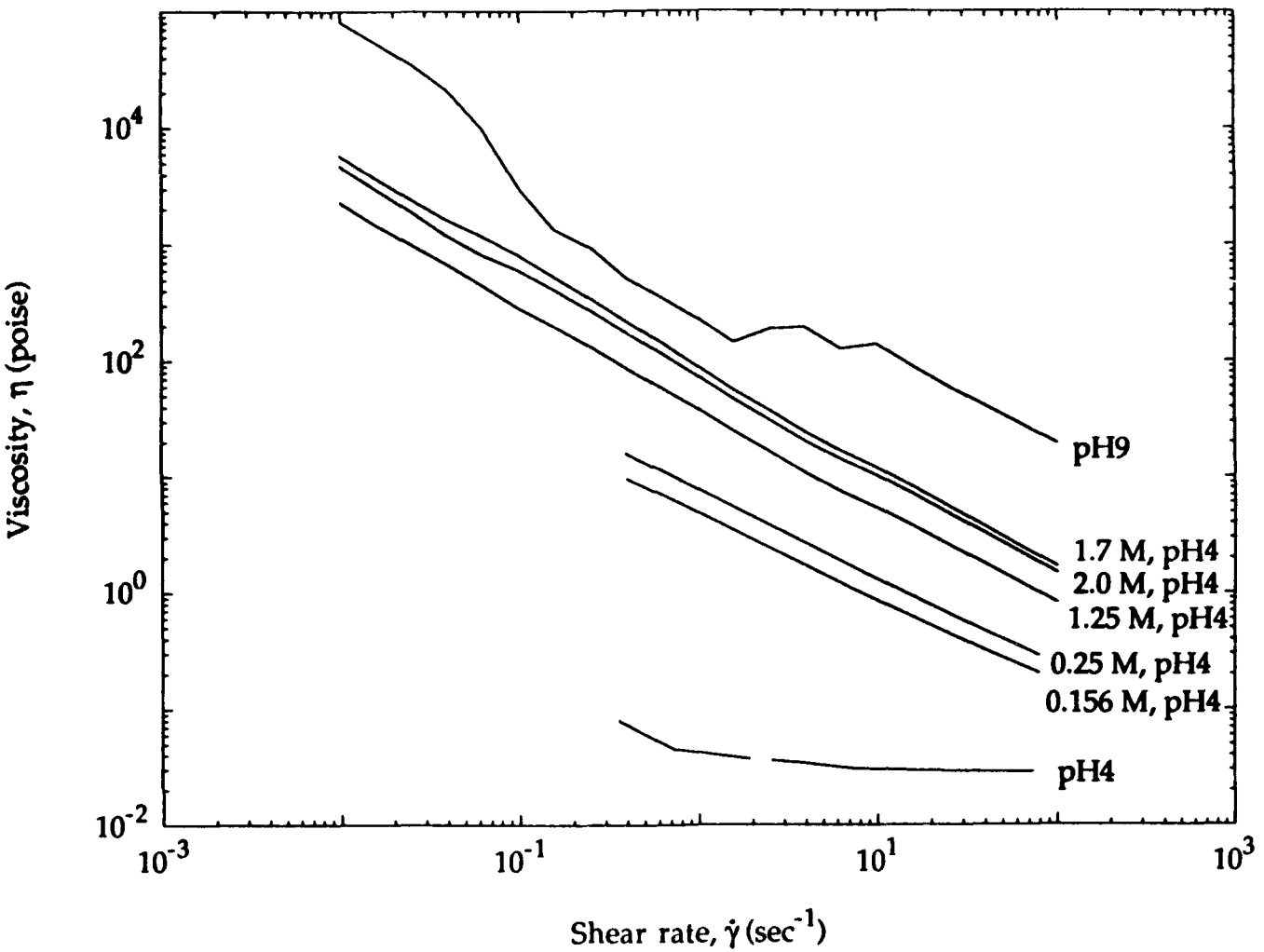
Viscosity, η (poise)
10^4
10^2
10^0
10^{-2}
10^{-3}
10^{-1}
10^1
10^3
Shear rate, $\dot{\gamma}$ (sec^{-1})
pH9
1.7 M, pH4
2.0 M, pH4
1.25 M, pH4
0.25 M, pH4
0.156 M, pH4
pH4

Figure 3a

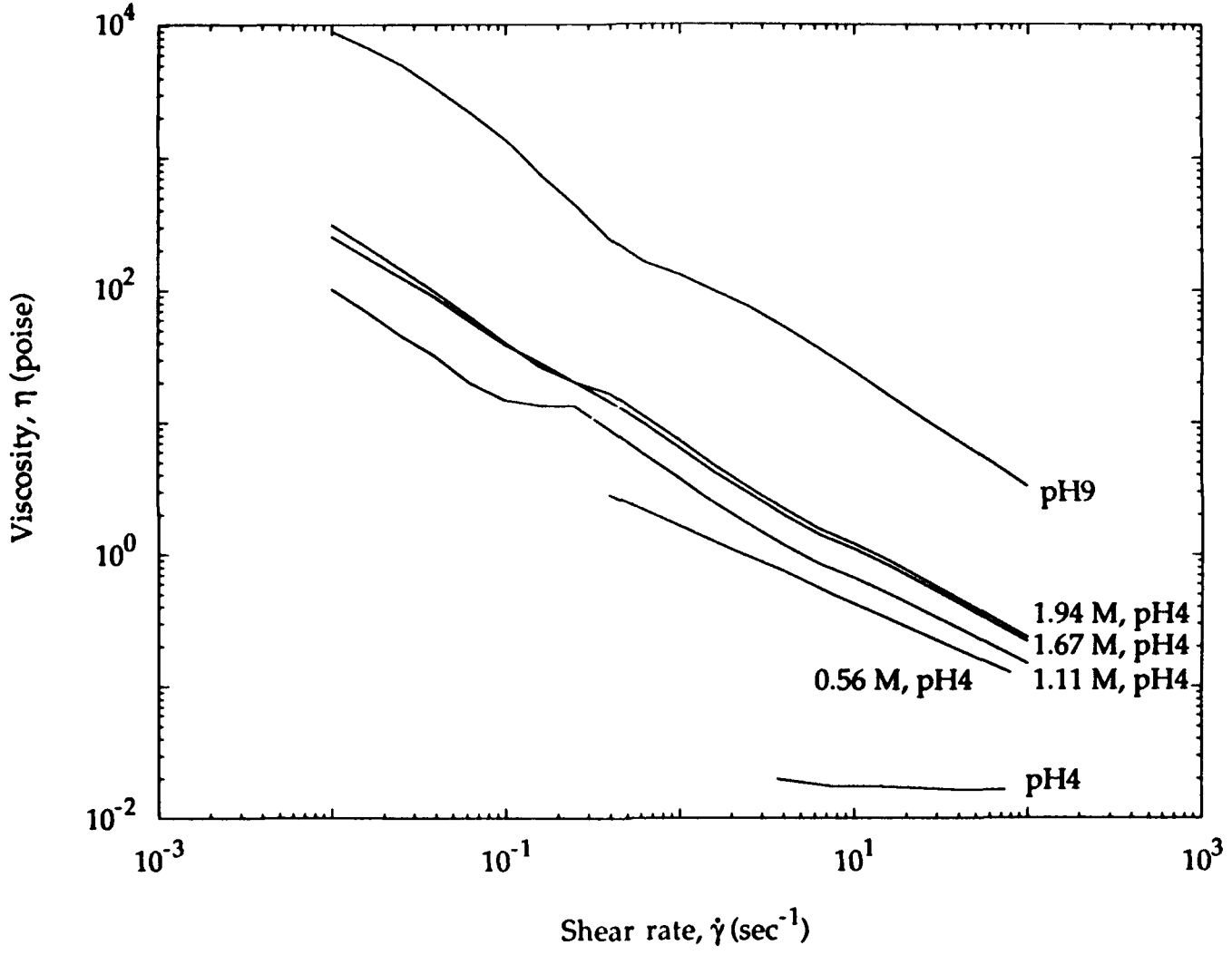
10^4
10^2
10^0
10^{-2}
10^{-3}
10^{-1}
10^1
10^3
Viscosity, η (poise)
Shear rate, $\dot{\gamma}$ (sec^{-1})
pH9
1.94 M, pH4
1.67 M, pH4
0.56 M, pH4
1.11 M, pH4
pH4

Figure 3c

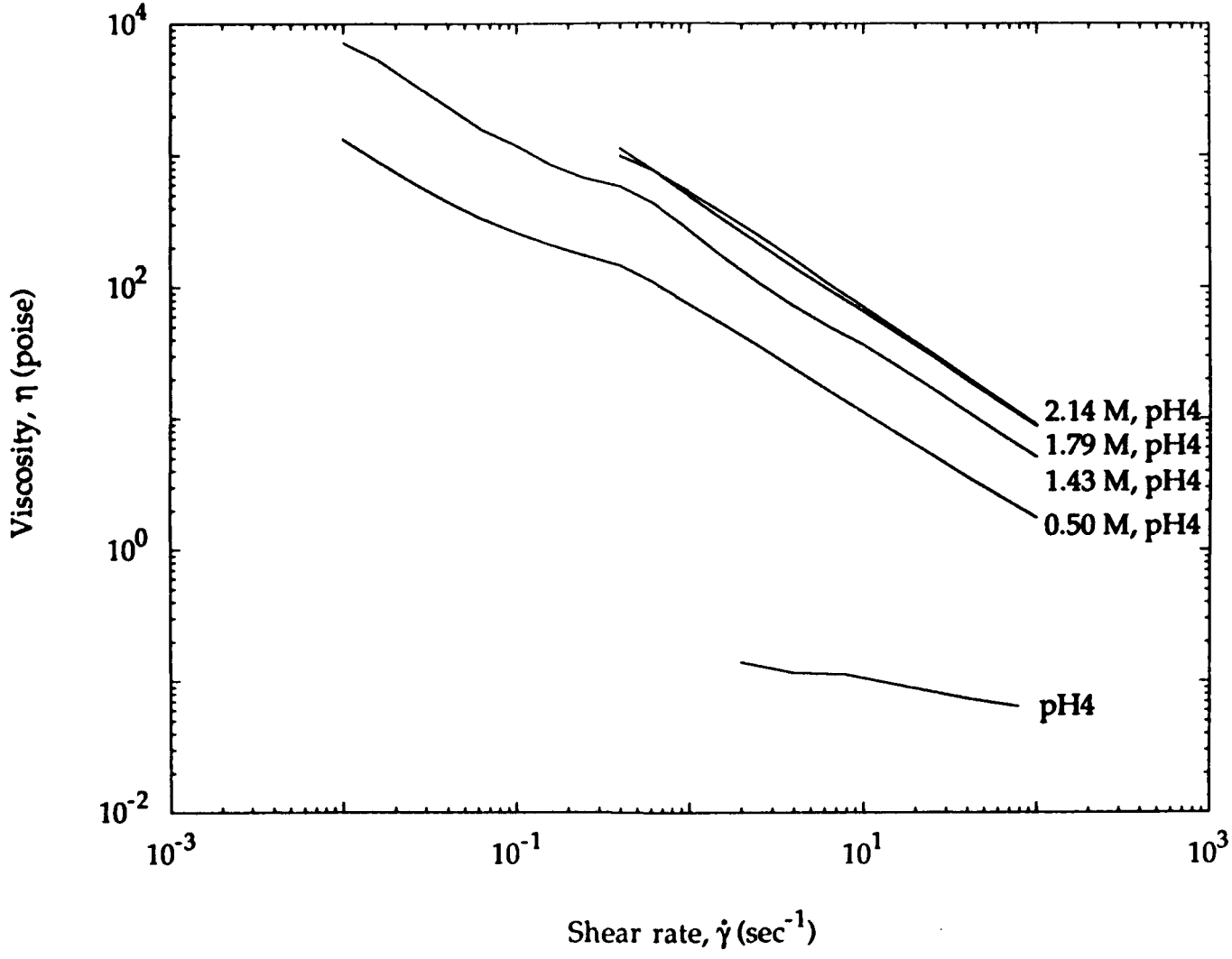
10^4
10^2
10^0
10^{-2}
Viscosity, η (poise)
10^{-3}
10^{-1}
10^1
10^3
Shear rate, $\dot{\gamma}$ (sec^{-1})
2.14 M, pH4
1.79 M, pH4
1.43 M, pH4
0.50 M, pH4
pH4

Figure 4

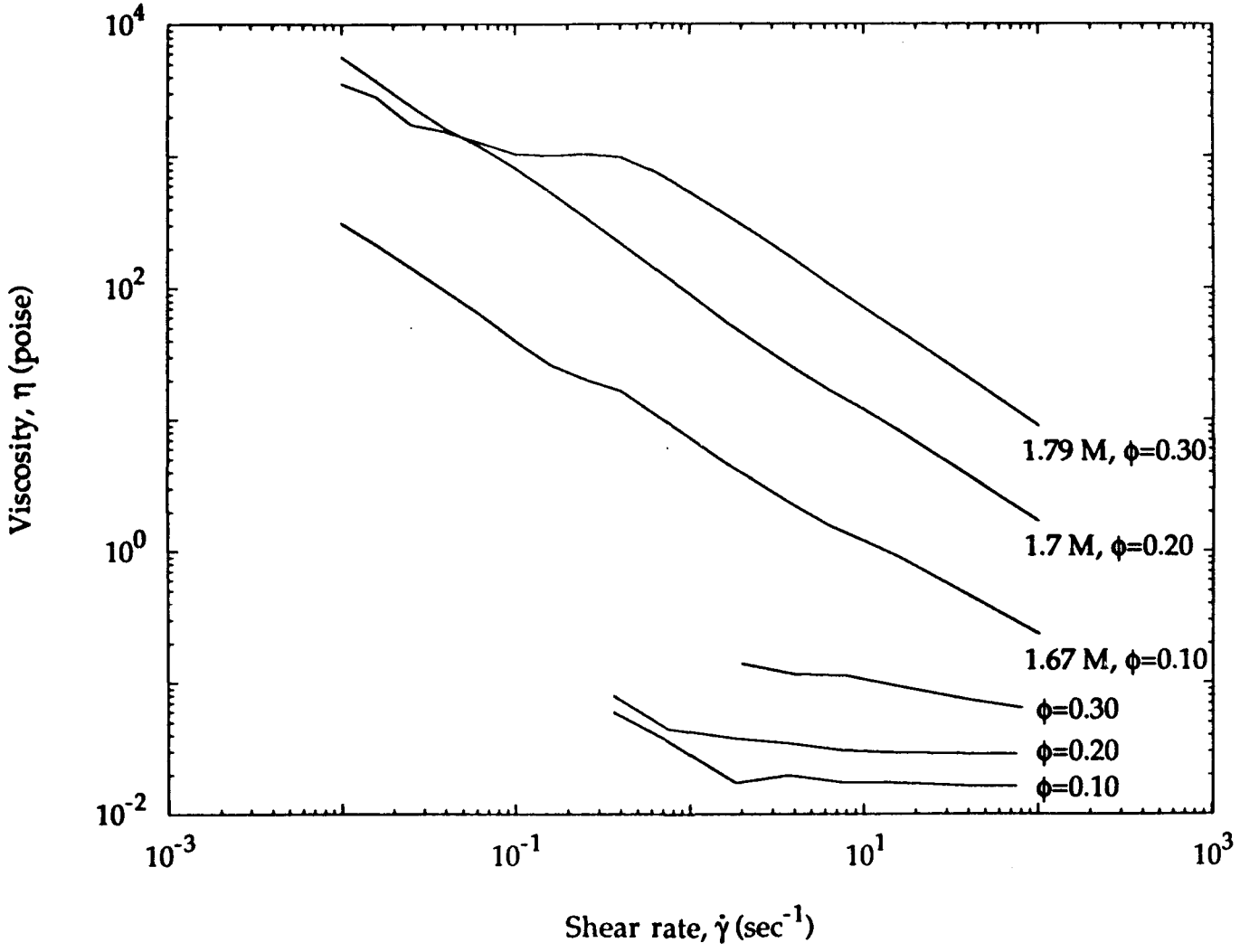
Viscosity, η (poise)
10^4
10^2
10^0
10^-2
10^-3
10^-1
10^1
10^3
Shear rate, γ̇ (sec^-1)
1.79 M, ϕ=0.30
1.7 M, ϕ=0.20
1.67 M, ϕ=0.10
ϕ=0.30
ϕ=0.20
ϕ=0.10

Figure 5

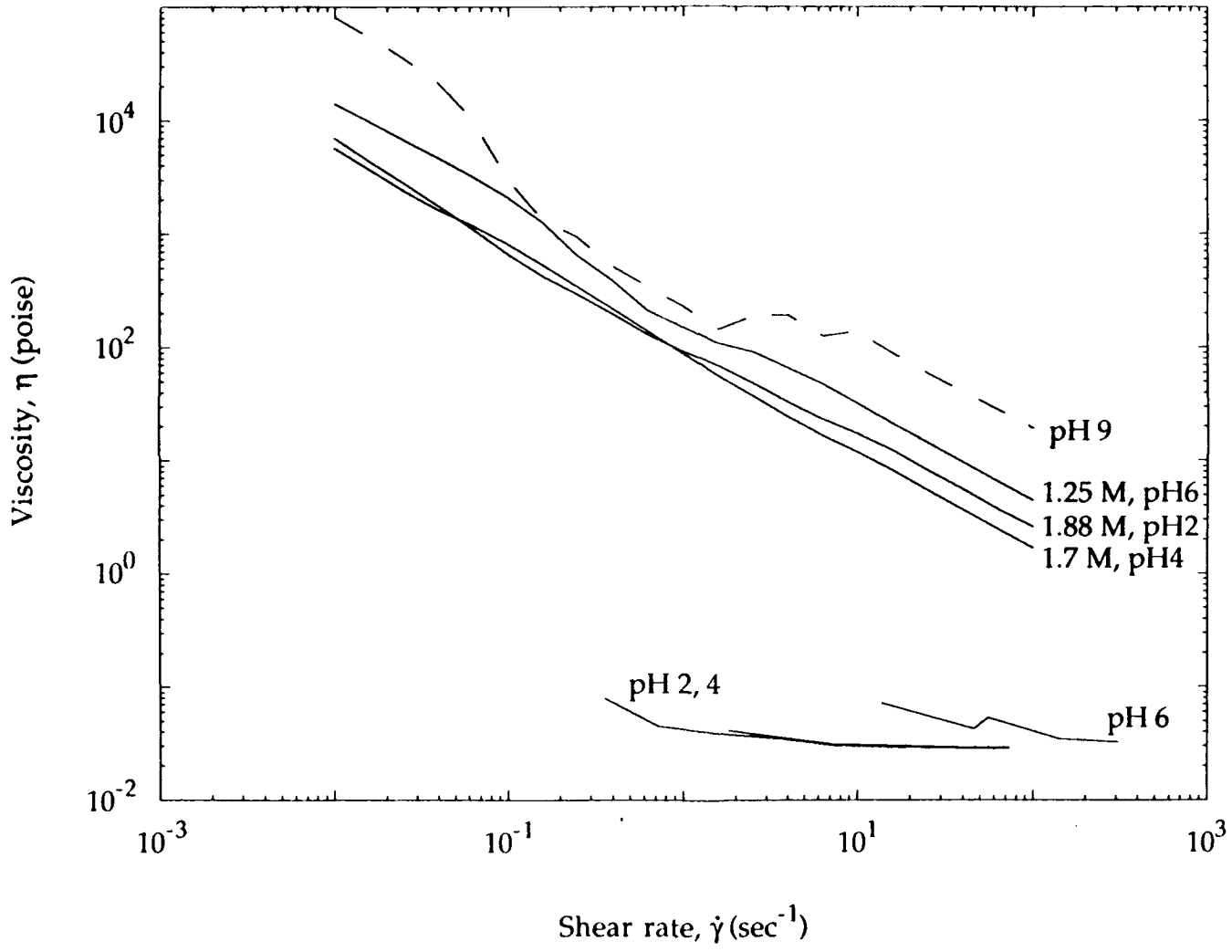
Viscosity, η (poise)
10^4
10^2
10^0
10^{-2}
10^{-3}
10^{-1}
10^1
10^3
Shear rate, $\dot{\gamma}$ (sec^{-1})
pH 9
1.25 M, pH6
1.88 M, pH2
1.7 M, pH4
pH 2, 4
pH 6

Figure 6

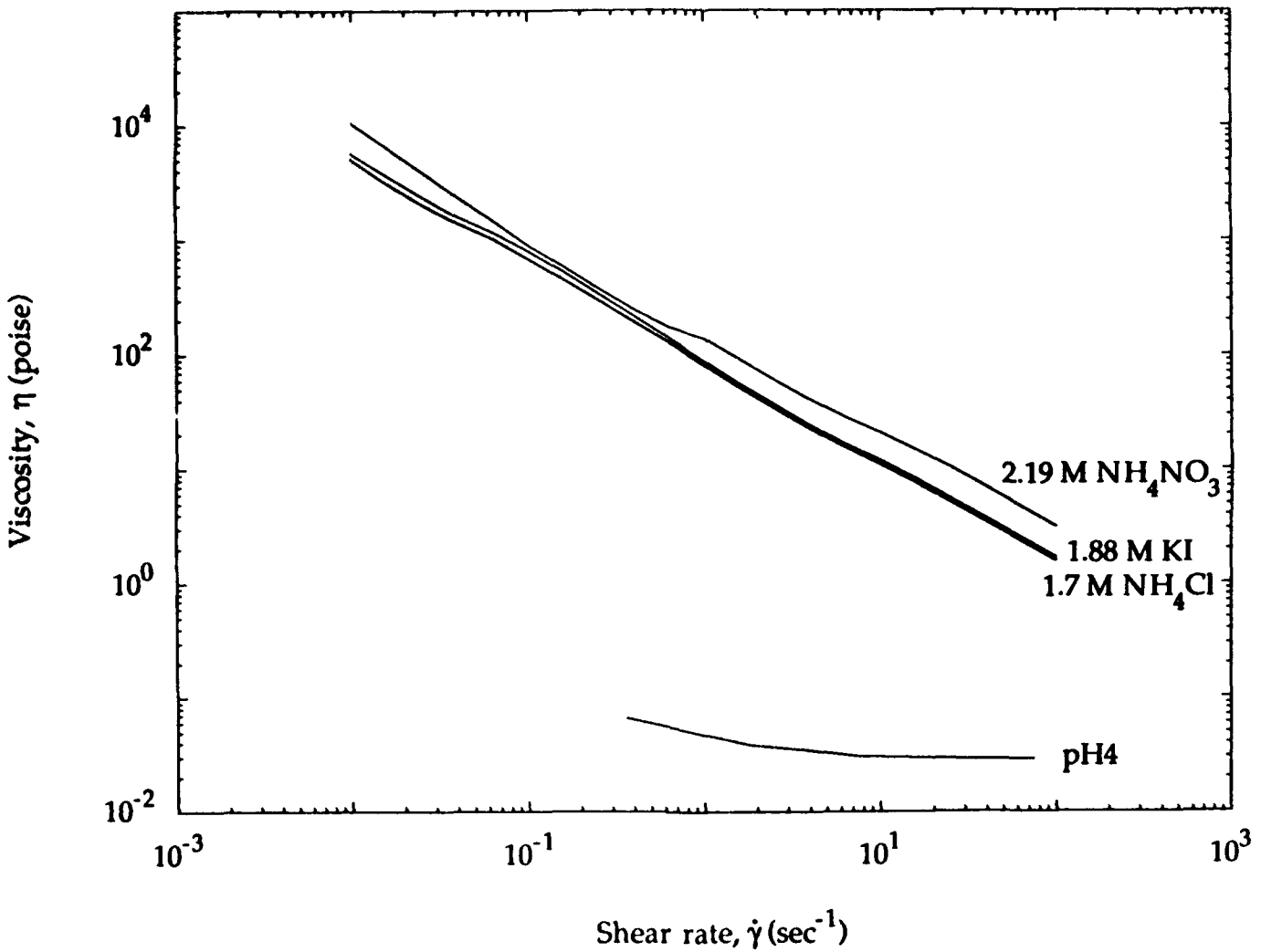
Viscosity, η (poise)
10^4
10^2
10^0
10^-2
10^-3
10^-1
10^1
10^3
Shear rate, γ̇ (sec^-1)
2.19 M NH4NO3
1.88 M KI
1.7 M NH4Cl
pH4

Figure 7

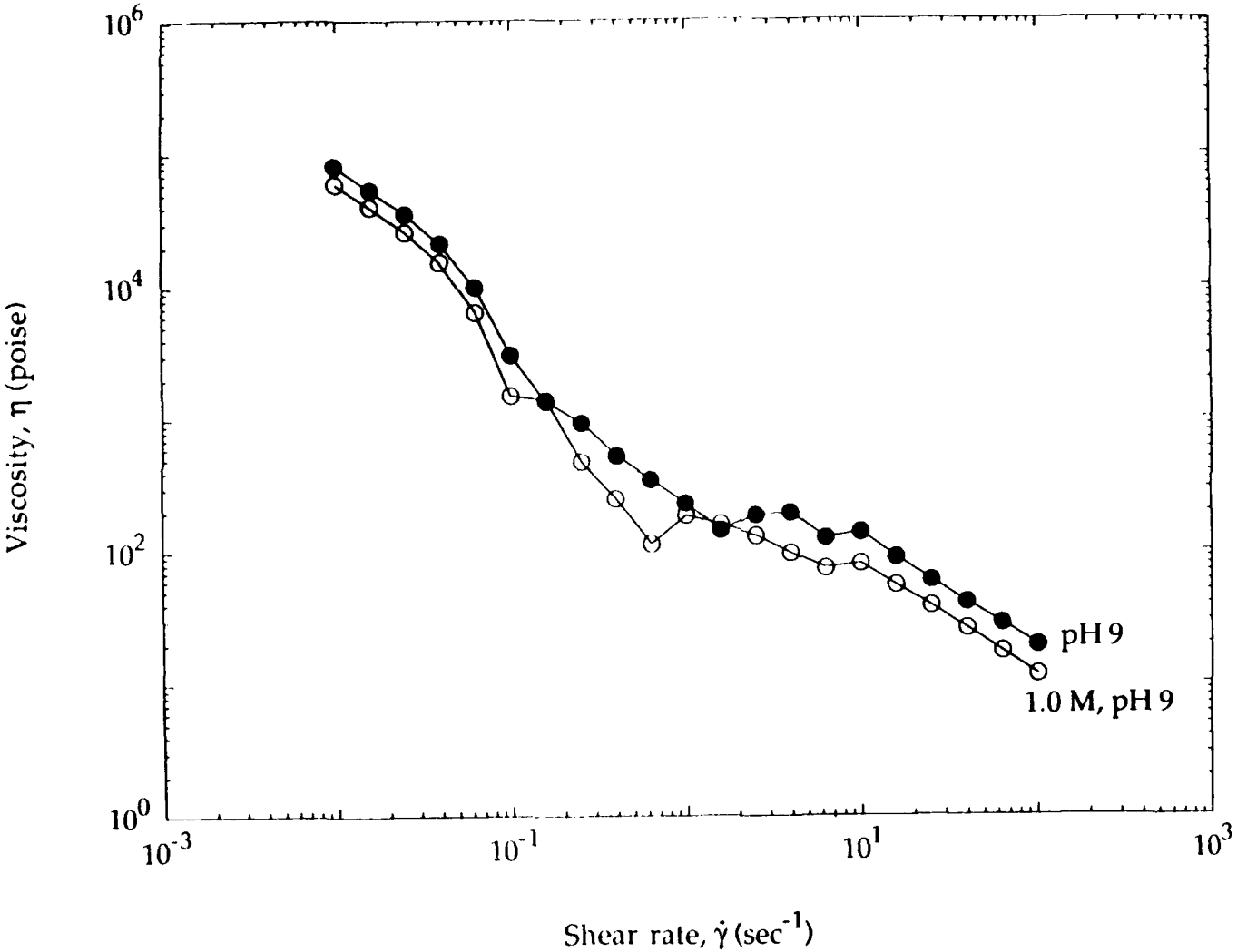
10^6
10^4
10^2
10^0
Viscosity, η (poise)
10^{-3}
10^{-1}
10^1
10^3
Shear rate, $\dot{\gamma}$ (sec^{-1})
pH 9
1.0 M, pH 9

Figure 8

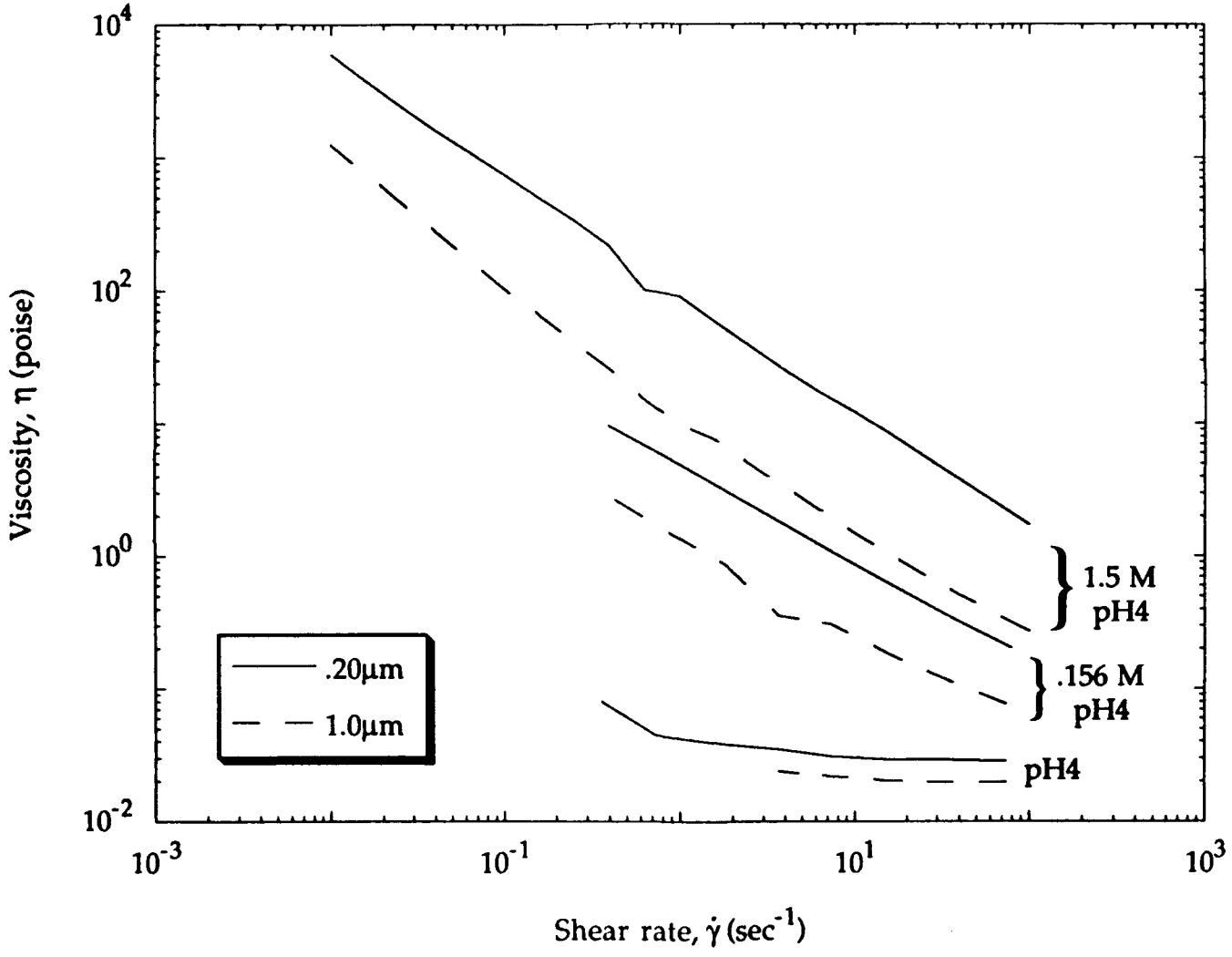
10^4
10^2
10^0
10^{-2}
Viscosity, η (poise)
10^{-3}
10^{-1}
10^1
10^3
Shear rate, $\dot{\gamma}$ (sec^{-1})
.20μm
1.0μm
1.5 M pH4
.156 M pH4
pH4

Figure 9a

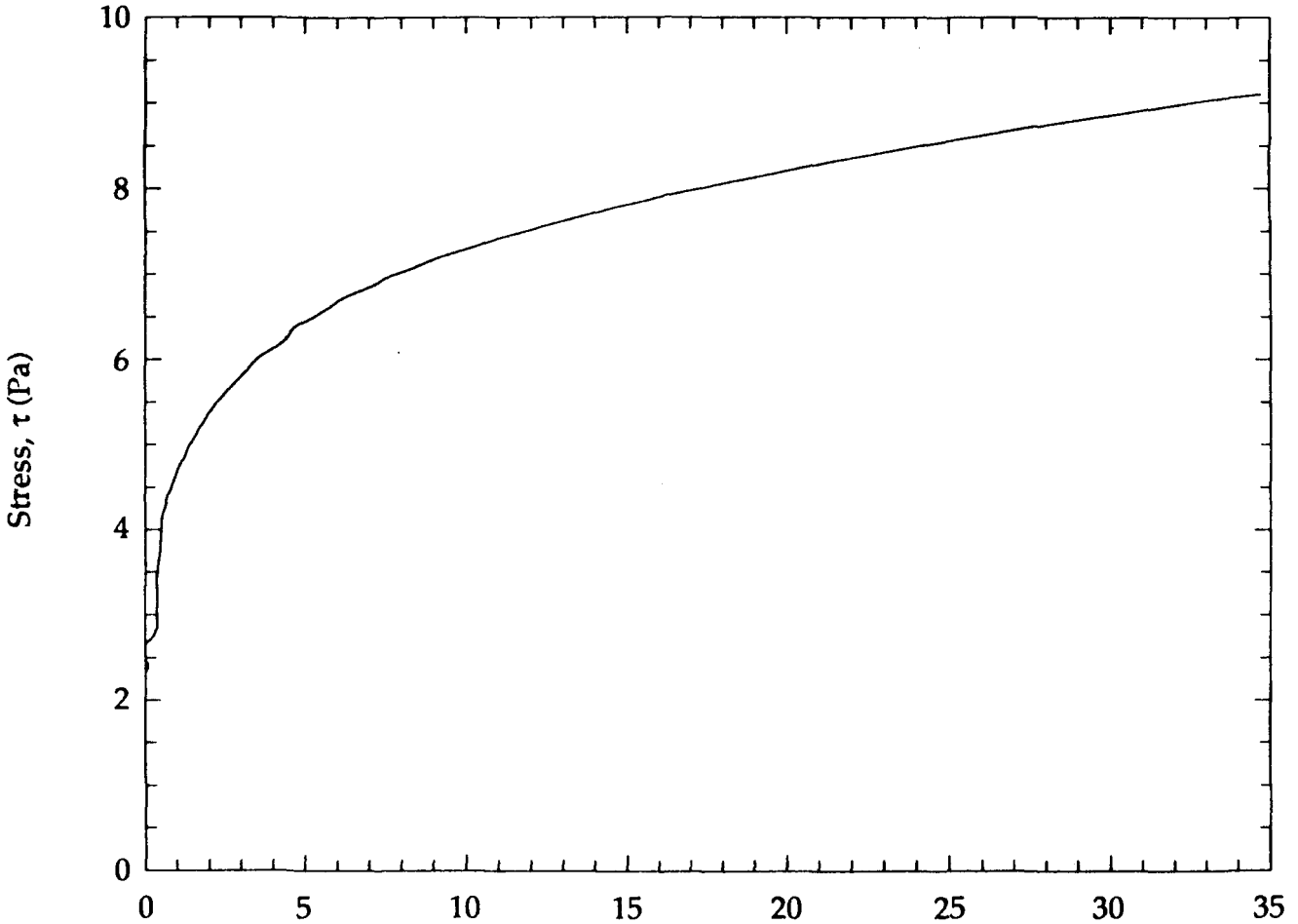

Figure 9b

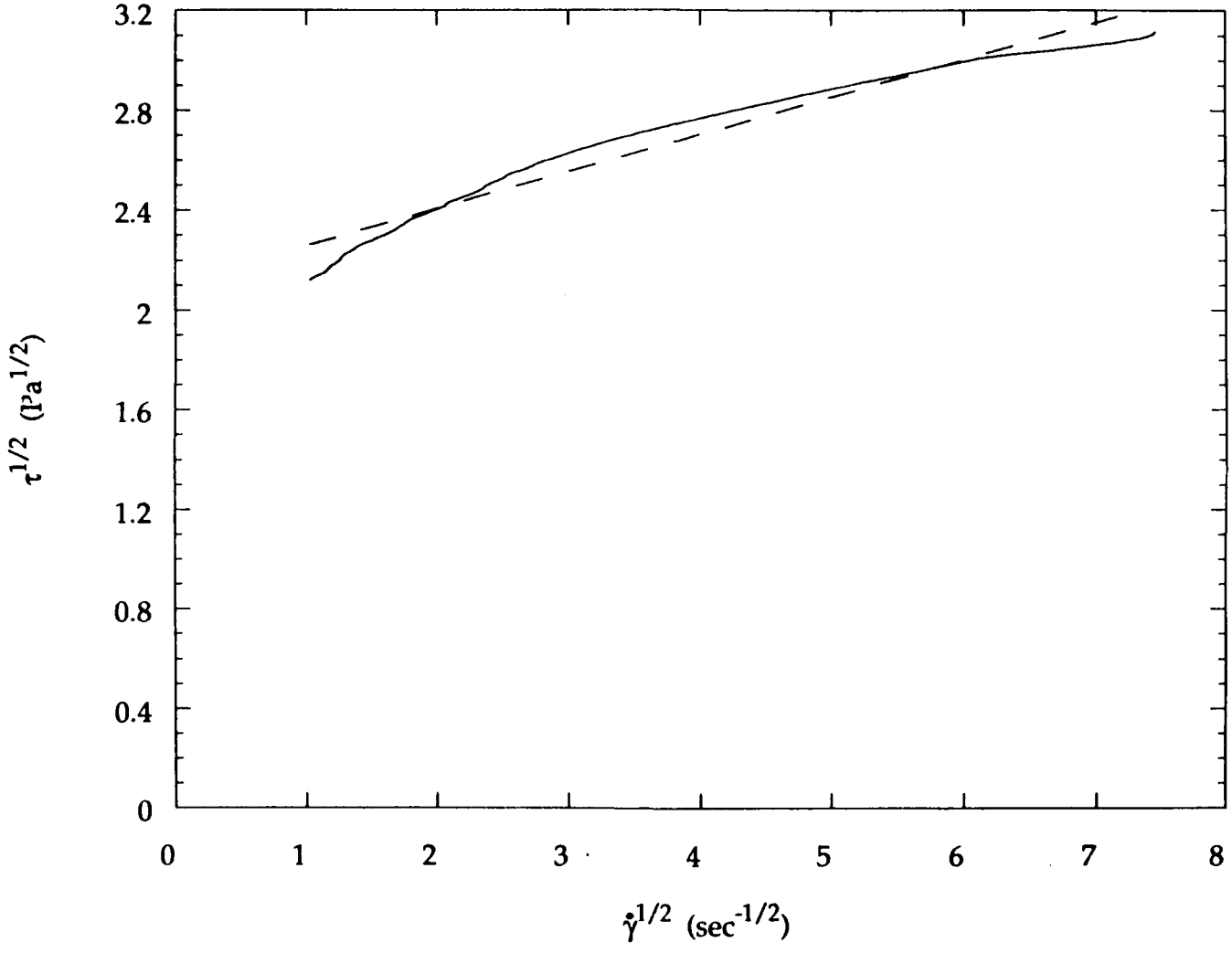

Figure 10

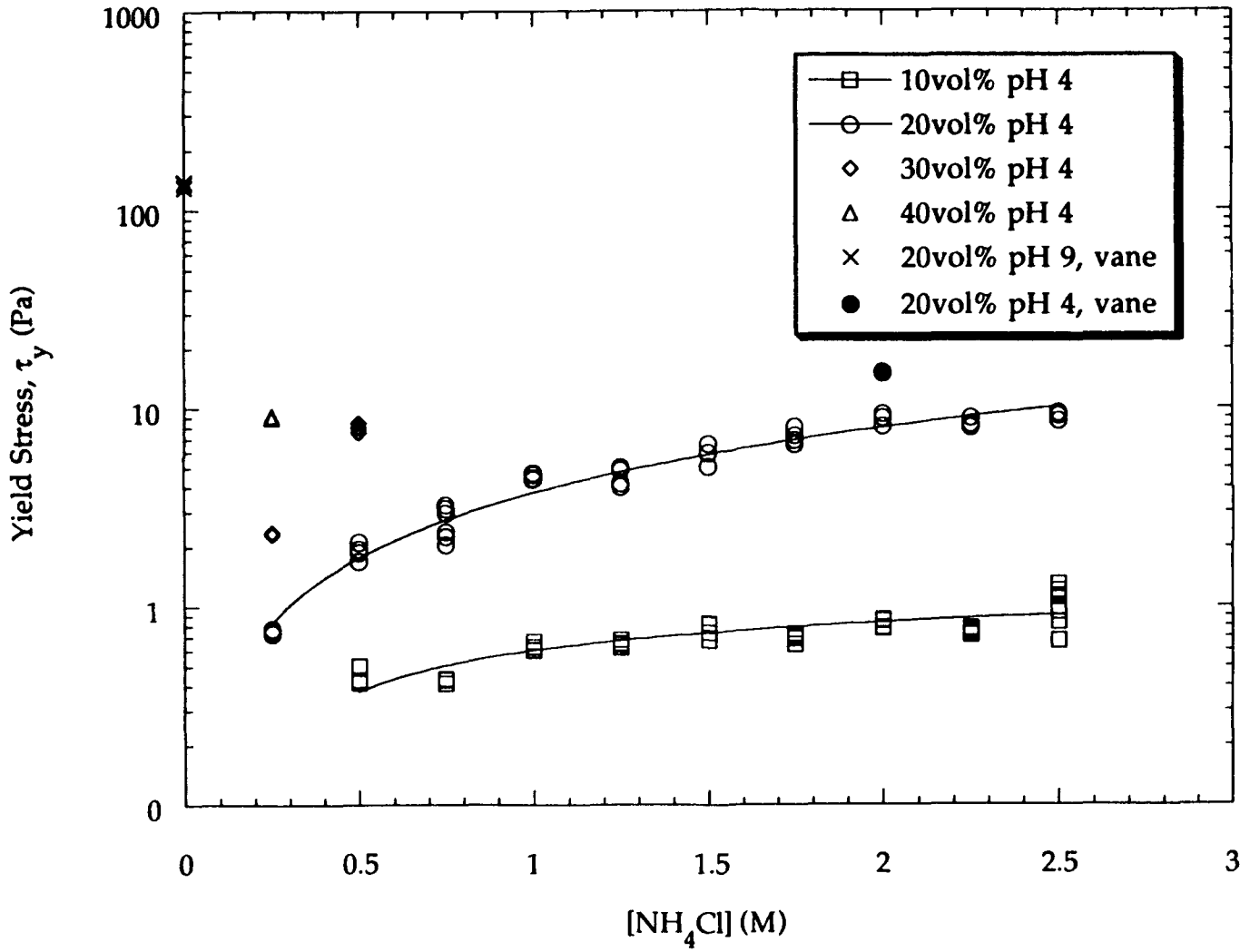
1000
100
10
1
0
Yield Stress, τ_y (Pa)
0
0.5
1
1.5
2
2.5
3
[NH_4Cl] (M)
10vol% pH 4
20vol% pH 4
30vol% pH 4
40vol% pH 4
20vol% pH 9, vane
20vol% pH 4, vane